

# A Nonparametric Bayesian Solution of the Empirical Stochastic Inverse Problem

Haiyi Shi<sup>1</sup>, Lei Yang<sup>2</sup>, Jiarui Chi<sup>3</sup>, Troy Butler<sup>4</sup>, Haonan Wang<sup>5</sup>,  
Derek Bingham<sup>6</sup>, and Don Estep<sup>7</sup>

<sup>1</sup>*Department of Statistics and Actuarial Science, Simon Fraser University, Burnaby, British Columbia V5A 1S6,  
e-mail: [haiyi\\_shi@sfu.ca](mailto:haiyi_shi@sfu.ca)*

<sup>2</sup>*Department of Statistics, Colorado State University, Fort Collins, Colorado 80537, e-mail:  
[yangleicq@gmail.com](mailto:yangleicq@gmail.com)*

<sup>3</sup>*Biostatistics and Programming, Sanofi, 55 Corporate Drive, Bridgewater, NJ 08807, e-mail:  
[Jiarui.Chi@sanofi.com](mailto:Jiarui.Chi@sanofi.com)*

<sup>4</sup>*Department of Mathematics and Statistics, University of Colorado at Denver, Denver, CO 80217, e-mail:  
[troy.butler@ucdenver.edu](mailto:troy.butler@ucdenver.edu)*

<sup>5</sup>*Department of Statistics, Colorado State University, Fort Collins, Colorado 80537, e-mail:  
[haonan.wang@colostate.edu](mailto:haonan.wang@colostate.edu)*

<sup>6</sup>*Department of Statistics and Actuarial Science, Simon Fraser University, Burnaby, British Columbia V5A 1S6,  
e-mail: [dbingham@sfu.ca](mailto:dbingham@sfu.ca)*

<sup>7</sup>*Department of Statistics and Actuarial Science, Simon Fraser University, Burnaby, British Columbia V5A 1S6,  
e-mail: [destep@sfu.ca](mailto:destep@sfu.ca)*

**Abstract:** The stochastic inverse problem is a key ingredient in making inferences, predictions, and decisions for complex science and engineering systems. We formulate and analyze a nonparametric Bayesian solution for the stochastic inverse problem. This paper presents a number of key results including; establishment of a unique nonparametric Bayesian posterior solution of the stochastic inverse problem corresponding to a chosen prior with an explicit formula for the corresponding conditional density; a maximum entropy property of the posterior solution corresponding to the uniform prior; the almost everywhere continuity of the density of the nonparametric posterior; and a comprehensive convergence and asymptotic analysis of a computational methodology based on a form of importance sampling. We illustrate the problem and results using several examples, including a simple experiment.

**MSC2020 subject classifications:** Primary 62G05, 65C60; secondary 62B99, 62P30, 62P35, 60D05, 60A10.

**Keywords and phrases:** disintegration of measures, generalized contours, importance sampling, random experiment, stochastic inverse problem.

## 1. Introduction

The behaviour of a complex system is governed by physical processes and laws, while the behaviour of any specific example of the system depends on its unique characteristics, or *parameters*, e.g., geometry, material properties, or rates of interaction. For instance, many materials respond to heat stress in similar ways, but the response of a particular object depends on factors such as its composition, thermal diffusivity, and shape.

In many real-world settings, parameters determining the behavior of a complex system cannot be measured directly. Instead, experiments typically produce observations of system behavior. To make sense of these observations, scientists and engineers rely on computer models that encode the mathematical representations of the governing physical laws to link parameters to observations. For example, the heat equation, a well-validated partial differential equation, describes how an object responds to a heat source. Measuring the object's temperature at a given time and location corresponds to evaluating the solution of this model, and from such measurements one can infer information about parameters related to the object's material composition such as thermal conductivity.

This gives rise to the general inverse problem where investigators infer the unknown parameters using a process model and observations. Solving this problem plays an important role in many applications, e.g., forecasting epidemics, designing new materials, assessing radiation damage in nuclear fuel rods, predicting climate and weather, detection of black holes, modeling subsurface contamination in aquifers, and estimating storm surge from hurricanes. There are many approaches to this inverse problem; see Sec. 1.4 for more details. We take a statistical approach in which the inferential object of interest is the distribution of parameters. Obtaining a distribution is a key ingredient for predicting system behavior.

### 1.1. The empirical stochastic inverse problem for random experiments

We begin by introducing the inverse problem and giving an overview of the main results. We assume that the parameters determining system behavior take values in a set  $\Lambda \subset \mathbb{R}^n$ ,  $n \geq 1$ . We consider the common situation in which it is not possible to observe the parameters directly. Instead, we assume that it is possible to observe data that corresponds to a function of the parameters. Specifically, we observe values of a vector or scalar function  $Q(\lambda)$  for any  $\lambda \in \Lambda$ , where  $Q : \Lambda \rightarrow \mathcal{D}$  with range  $\mathcal{D} = Q(\Lambda) \subset \mathbb{R}^m$  for  $m \leq n$ .  $Q$  is called the **quantities (quantity) of interest (QoI)**.

In many cases, defining the QoI is key to experimental design. As with the heat equation,  $Q(\lambda) = q(Y(\lambda))$  is typically obtained by applying a **observation map**  $q$  to the solution  $Y$  of a **process model**  $\mathcal{M}(Y, \lambda) = 0$  that encapsulates physical properties, e.g., conservation of mass and energy, where  $Y$  is an implicit function of the physical parameters  $\lambda \in \Lambda$ . An important issue is that  $Q$  is generally not 1 – 1, which reflects the loss of information in experimental observations. In this case, multiple physical instances, i.e., values of  $\lambda$ , yield the same set of experimental data. It turns out that this is directly related to the introduction of conditional probability.

In many applications in science and engineering, it is natural to use a probability model for the physical parameters. One common situation is a parameter that varies naturally and is modeled as stochastic. For example, the temperature applied during an experiment of heating an object varies from trial to trial. Another common situation is the case where a parameter represents “up-scaled” behavior of system or quantity that varies in a complex fashion, at a rapid time scale, and/ or small spatial scale. In the heat equation, the thermal conductivity parameter represents an upscaled representation of the behavior of the molecules in the object under study [76]. In many cases, such upscaled behavior can be described by a probability model with high fidelity [4]. Another important application of a probability model is as a framework for uncertainty when a parameter value is unknown.

The **probability model for the parameters** is defined as  $(\Lambda, \mathcal{B}_\Lambda, P_\Lambda^d)$  where  $\Lambda$  is a Borel-measurable set that determines the relevant physical range, the Borel  $\sigma$ -algebra  $\mathcal{B}_\Lambda$  describes how information about the values of the physical parameters is quantified, and the probability distribution  $P_\Lambda^d$  describes the variation in parameter values. We assume that  $Q : (\Lambda, \mathcal{B}_\Lambda) \rightarrow (\mathcal{D}, \mathcal{B}_\mathcal{D})$  is a random vector, where  $\mathcal{B}_\mathcal{D}$  is the restriction of the Borel  $\sigma$ -algebra to the observation space  $\mathcal{D}$ .

$Q$  induces the **induced** or **push-forward** probability measure  $P_\mathcal{D}$  on  $(\mathcal{D}, \mathcal{B}_\mathcal{D})$  defined,

$$P_\mathcal{D}(A) = QP_\Lambda^d(A) = P_\Lambda^d(Q^{-1}(A)), \quad A \in \mathcal{B}_\mathcal{D},$$

where the inverse is defined,

$$Q^{-1}(A) = \{\lambda \in \Lambda : Q(\lambda) \in A\}, A \in \mathcal{B}_\mathcal{D}.$$

For any  $q \in \mathcal{D}$ , the **generalized contour**  $Q^{-1}(q)$  gives all possible input parameter values  $\lambda$  that result in the same output. It is the generalization of a contour curve for a scalar map on two dimensions. Because  $\mathcal{D}$  is the range of  $Q$ , we obtain the decomposition  $\Lambda = \bigcup_{q \in \mathcal{D}} Q^{-1}(q)$ , where  $Q^{-1}(q_1) \cap Q^{-1}(q_2) = \emptyset$  when  $q_1 \neq q_2$ . Below, we investigate the properties of generalized contours that are important for the practical use of conditional probability.

We now have the ingredients for the classic model of a random experiment. Given data  $\{q_i\}_{i=1}^K$  for  $K$  trials of the experiment, we assume that there is a collection of  $K$  parameter values  $\{\lambda_i\}_{i=1}^K$  that are distributed according to  $P_\Lambda^d$  such that  $q_i = Q(\lambda_i)$  for  $1 \leq i \leq K$ . The collection of data  $\{q_i\}_{i=1}^K$  is distributed according to  $P_\mathcal{D}$ . We define the stochastic inverse problem in the situation that  $P_\Lambda^d$  is unknown. In this context,  $P_\Lambda^d$  is called the **data generating distribution**.

**Definition 1.1 (empirical Stochastic Inverse Problem (eSIP)).** Determine a probability distribution  $P_\Lambda$  on  $(\Lambda, \mathcal{B}_\Lambda)$  such that any collection of observations  $\{q_i\}_{i=1}^K$  of  $Q$  (distributed according to  $P_\mathcal{D} = QP_\Lambda^d$ ) is a random sample from the induced probability distribution  $P_\mathcal{D} = QP_\Lambda$ .

The eSIP has multiple solutions when  $Q$  is not 1 – 1. We adopt a Bayesian approach to determine a unique solution of the eSIP conditioned on a prior distribution that encapsulates prior information about the physical system.

There are many applications where characterizing the distribution of the input parameters to a computer model is an important scientific goal. For example, the distribution of near shore bathymetry is estimated from a computer model for the shallow water equations and wave data obtained from buoys in [12]. The distribution on the concentration of a contaminant at the source of groundwater pollution is estimated from data on concentrations at wells located at some distance from the source using a computer model of contaminant transport in [53]. In [13, 36], the distribution on the Manning's  $n$  parameter field quantifying bottom friction in computer models of hydrodynamics is estimated from wave data obtained from buoys. In [38], experimental data and computer model simulations are used to characterize the impurity concentration in graphite bricks used in nuclear reactors. In [52], an emulator for the mass expelled (*chirp mass*) during binary black hole mergers is combined with gravitational wave data to estimate the distribution of parameters including masses of stars in binary systems and initial orbital separation of the stars that evolve into black hole mergers.

The thermal diffusivity of protein and bone in cooking steaks is estimated from temperature data and a computer model for the heat equation in [6]. A computer model for muon radiation scattering and data obtained from muon radiation detectors is used to estimate the distribution of the possible location of a subsurface critical mineral deposit in [75] and the distribution on the possible geometry of an air gap in a block cave mine in [7]. In [47], distribution of rate parameters in a computer model of a COVID-19 “surge” is estimated using data of changes in the susceptible population.

We develop the foundational theory for existence and fundamental properties of the solution of the eSIP using an abstract version:

**Definition 1.2 (Stochastic Inverse Problem (SIP)).** Given the induced distribution  $P_{\mathcal{D}} = QP_{\Lambda}^d$  on  $(\mathcal{D}, \mathcal{B}_{\mathcal{D}})$ , compute a probability distribution  $P_{\Lambda}$  on  $(\Lambda, \mathcal{B}_{\Lambda})$  such that  $P_{\mathcal{D}}(\cdot) = QP_{\Lambda}$ .

We return to consider the eSIP when developing the computational solution methodology in Sec. 3.

## 1.2. An overview of the main results

We summarize the main results in this paper. The details are developed in the coming sections.

**Main result 1** Assume that  $P_{\mathcal{D}}$  has density  $\rho_{\mathcal{D}}$  with respect to Lebesgue measure. Under general conditions, for each prior distribution  $P_p$  on  $(\Lambda, \mathcal{B}_{\Lambda})$  with density  $\rho_p$  there is a unique posterior distribution  $P_{\Lambda}$  that solves the SIP and there is an explicit formula for its density  $\rho_{\Lambda}$  determined from  $\rho_{\mathcal{D}}$  and  $\rho_p$ . This is the nonparametric analog of the result typically deployed for classic Bayesian statistics.

**Main result 2** Under general conditions, the density  $\rho_{\Lambda}$  of the Bayesian solution of the SIP is continuous a.e.

**Main result 3** Under general conditions, the Bayesian solution of the SIP corresponding to the uniform prior has maximum entropy.

**Main result 4** Returning to the eSIP, we construct a numerical estimate  $\hat{P}_{\Lambda} \approx P_{\Lambda}$  based on a form of importance sampling. Under general conditions, the estimator  $\hat{P}_{\Lambda}$  is asymptotically unbiased and strongly consistent and we provide asymptotic estimates of its variance and error.

Broadly speaking, the first result says that even for complex computer models, there exists a unique posterior distribution to the SIP with an explicit formula for the density. The second result implies that the posterior distribution is well-behaved in practical settings. The third main result says that under general conditions that the uniform prior is the least informative choice. Finally the fourth main result is that there is a robust, reliable, and practical numerical solution methodology.

**Example 1.** To illustrate the ideas to be developed, we consider a model for exponential decay that has some of the main features encountered in practice. The model is,

$$\begin{cases} \frac{dy}{dt} = -\lambda_2 y, & 0 < t \leq T, \\ y(0) = \lambda_1, \end{cases} \quad (1.1)$$

where we treat the initial condition and the rate as unknown. The quantity of interest is the value of the solution at time  $T$ :  $Q(\lambda_1, \lambda_2) = y(T) = \lambda_1 \exp(-\lambda_2 T)$ . We set  $\Lambda = [0, 1] \times [0, 1]$  and  $\mathcal{D} = [0, 1]$ .

**Remark 1.3.** This example illustrates the common situation in which the QoI depends on auxiliary variables such as time and spatial location. In this case, choosing two different times yields two different QoI. But, there may be a strong dependency on a QoI evaluated at two times or at nearby spatial points. This is explored in [13, 47, 66].

In Fig. 1, we plot 32 generalized contours  $Q^{-1}(q)$ , where the contour corresponding to an observed value  $q \in [0, 1]$  is defined by  $\lambda_1 = q \exp(T \lambda_2)$  for  $0 \leq \lambda_2 \leq 1$ . The surface length of the contours depends on the geometry of the boundary of  $\Lambda$  as well as the time  $T$  of observation. To generate *synthetic data*, we assume a data generating distribution  $P_{\Lambda}^d$  of

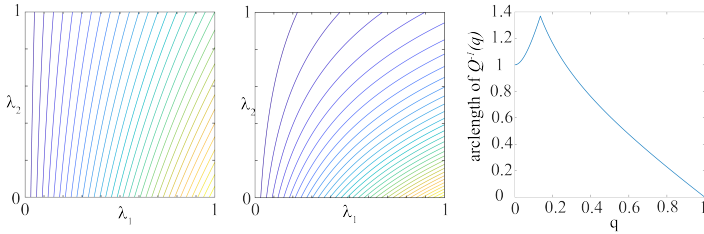


Fig 1. We show 32 generalized contours for the map  $Q$  for the exponential decay model in Example 1 corresponding to  $T = .5$  (left) and  $T = 2$  (center). Each contour curve corresponds to a different value of  $q$ . On the right, we plot the arclength of the generalized contours  $Q^{-1}(q)$  against  $q$  for  $T = 2$ .

independent Beta (12, 12) distributions for  $\lambda_1$  and  $\lambda_2$ . We draw samples from  $P_{\Lambda}^d$  and evaluate the solution at time  $T$  at the samples to generate observed data. We plot empirical densities for  $P_{\Lambda}^d$  and the corresponding output distributions  $P_{\mathcal{D}}$  at  $T = .5$  and  $T = 2$  using 200,000 samples in Fig. 2.

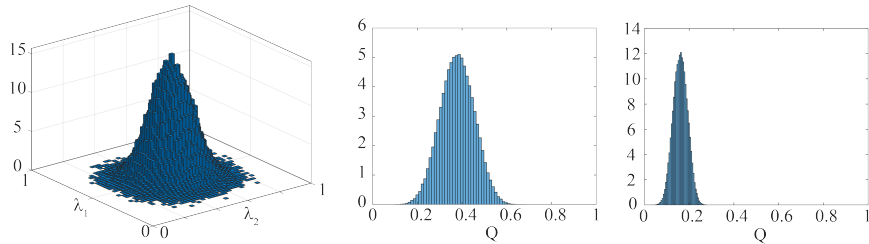


Fig 2. Left: empirical density for  $P_{\Lambda}^d$  for Example 1 computed using 200,000 points. Center: empirical density for  $P_{\mathcal{D}}$  at  $T = .5$ . Right: empirical density for  $P_{\mathcal{D}}$  at  $T = 2$ .

We compute the posterior distribution solving the eSIP with the uniform prior using the numerical solution method presented in Sec. 3 with a large number of samples in order to virtually eliminate effects of finite sampling. We sample  $16 \times 10^6$  points in  $\Lambda$  randomly from  $P_{\Lambda}^d$ . We use the synthetic data to build an empirical output distribution on a partition of  $\mathcal{D}$  with 100 cells. By a *partition* of a measurable set  $A$ , we mean a finite or countable collection of non-intersecting measurable subsets  $\{B_i\}_i$  such that  $A = \bigcup_i B_i$ , except possibly for set of

measure 0. We compute an empirical solution of the eSIP using  $16 \times 10^6$  uniformly distributed points in  $\Lambda$ .

In Fig. 3, we plot heatmaps of the eSIP solutions for  $T = .5$  and  $T = 2$  produced by computing  $\{P_\Lambda(B_i)\}_{i=1}^{6400}$  for a partition  $\{B_i\}_{i=1}^{6400}$  of  $\Lambda$  into small cells  $B_i$  and generating a heatmap from the probabilities. Recalling the contours shown in Fig. 1, the solutions have the characteristic “ridge” shape oriented along contours that reflects the fact that parameter values on the same contour have equal probability due to the choice of the uniform prior. This reflects the *indeterminacy* induced by the loss of information in the experimental observation. Note that we do not expect to recover the data generating distribution. We compute a posterior solution of the SIP conditioned on the choice of prior.

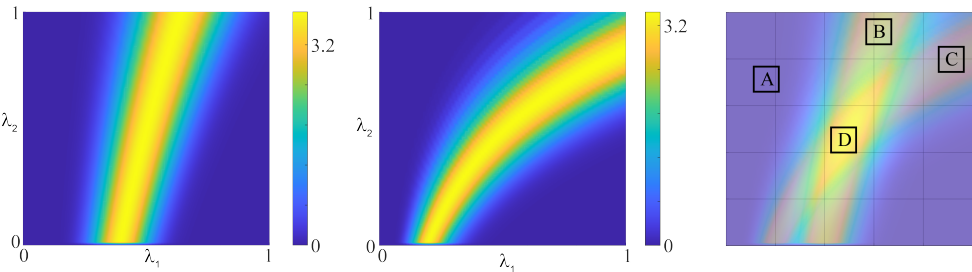


Fig 3. Left and center: Heatmaps of solutions of the eSIP for the exponential decay model using the uniform prior for  $T = .5$  (left) and  $T = 2$  (center). Right: Overlays of the two heatmaps. Event A is relatively low probability for both solutions, Event B is relatively high probability for the solution for time .5 but relatively low probability for the solution for time 2, while Event C is the reverse. Event D is relatively high probability for both solutions.

### 1.3. Using the solution of the eSIP

In applications of the eSIP, the principal inferential target is information about the probability of combinations of parameters consistent with the model and the observations. The solution of the eSIP is a posterior probability distribution on the sample space  $\Lambda$  that is evaluated to estimate probabilities of events. For example in the right hand plot in Fig. 3, we show four events of equal size located in different parts of  $\Lambda$ . We see that event A has relatively low probability with respect to the eSIP solutions for  $T = .5$  and  $T = 2$ , while event D has relatively high probability for both eSIP solutions. Events B and C are relatively high probability for one of the eSIP solutions but not the other.

**Remark 1.4.** We emphasize that the solution of the eSIP is a posterior probability distribution, not a point estimate. We can compute statistics of the posterior such as a mean or variance but those are typically of little use.

The ability to remove parts of  $\Lambda$  from consideration due to relatively low probability is often useful. It is also useful to identify the region of relatively high probability by marking cells in a partition whose probabilities are above a set threshold.

The other use of the solution of the eSIP is forecasting or prediction, which means computing a probability distribution on a new quantity of interest. For example, we can compute the solution of the eSIP for observations at an early time, then use the solution to estimate

the induced distribution on the quantity of interest at a later time. This is related to ensemble forecasting, see [47] for an example of forecasting infections of COVID during a surge using real data.

#### 1.4. Observations and related work

The data for the eSIP results from conducting trials of the experiment multiple times, with each trial conducted with physical parameters distributed according to an unknown data generating distribution. The eSIP is closely related to ensemble forecasting, e.g., as used in weather prediction [1, 27, 35, 47, 49, 50, 51, 56]. The stochastic variation in output data is the result of random sampling of the physical parameters rather than from observational noise. Thus, the eSIP is significantly different than the common statistics problem in which stochastic data results from noisy evaluation of an experiment conducted for a single set of parameters (a “true” value). Observational error can be added to the eSIP, and more generally, the eSIP can be extended to include random effects, but this increases the complexity and dimension of the inverse problem to be solved [5].

The inferential target of the eSIP is a probability distribution on the physical parameters as opposed to a distribution on parameters in a distributional model in a classic application of Bayesian statistics. The sample space  $\Lambda$  commonly includes ranges of values that lead to significantly different behavior in the system, e.g.,  $\Lambda$  may include bifurcation points. The distribution of the QoI is correspondingly complex. In general, the solution of the eSIP is a probability distribution with a complex heterogeneous structure, motivating the use of a nonparametric approach to computing approximate solutions.

The solution depends on disintegration of measures rather than an application of Bayes theorem [4, 8, 21, 34, 42, 44, 59, 64]. The regular conditional probability resulting from conditioning on the  $\sigma$ -algebra induced by  $Q$  plays a prominent role in the construction of the Bayesian solution of the eSIP. This reflects the fact that the experimental data provides limited information about the physical parameters.

Bayesian computer model calibration is a statistical approach that combines experimental data and computer model output to estimate a “true” value for the parameters (“calibration parameters”) in the presence of uncertainty [7, 38, 39, 40, 45, 52, 58, 71, 75]. Bayesian calibration typically employs an “emulator” (a statistical surrogate model for the computer model) and often attempts to model the systematic “discrepancy” between the calibrated model emulator and the mean of the physical system. The work in [38], for example, considers an inverse problem similar to the eSIP.

A related inverse problem involves the case where there is a single “true” value of the parameter. A stochastic approach widely employed in engineering [19, 24, 28, 31, 67, 69, 70] is the Bayesian Inverse Problem. This approach involves the introduction of observational noise and regularization. A variation arises when longitudinal data for a single parameter value is available, e.g., 4D-VAR, data assimilation, ensemble Kalman filtering, Bayesian particle filtering, et cetera [1, 2, 3, 20, 23, 26, 30, 30, 33, 62, 72]. These approaches also involve the introduction of random noise and regularization. In both cases, the problems and solution approaches are very different than the eSIP and our approach. The review paper [6] explores the relationship between the eSIP and the Bayesian Inverse Problem.

The original development of the SIP used a different form of disintegration and employed a deterministic numerical solution method [9, 11, 12]. This paper introduces a new form of disintegration of the solution that enables derivation of some key properties for the first time as well as analysis of a novel numerical solution method based on random sampling. The advances presented in this paper depend on the developments in the theses [22, 74]. Extensions of the eSIP to other problems are considered in [17, 22, 54, 74]. Consideration of computational aspects of the solution of the eSIP are considered in [15, 16, 18, 66, 77, 78]. Applications of the eSIP can be found in [10, 13, 14, 36, 43, 47, 53]. In traditional inverse problems, “ill-conditioning” and the condition number play important roles. In [66], we develop a theory of condition for the eSIP and explore the consequences for the solution. In [5], we consider the inclusion of random effects in the eSIP, which opens up doors to numerous applications and extensions, including connecting the eSIP to traditional Bayesian statistics.

### 1.5. Outline of the paper

In Sec. 2, we develop the formulation of the Bayesian solution of the SIP using disintegration of measures. We describe conditions that guarantee the solution can be expressed in terms of a conditional density in Sec. 2.4. We describe the maximum entropy property of the solution corresponding to the uniform prior in Sec. 2.5. In Sec. 2.6, we describe the continuity property of the solution. In Sec. 3, we describe and analyze the numerical solution method for the eSIP based on reweighting of random samples. In Sec. 4, we present two examples. We develop an alternative accept-reject numerical solution method in Sec. 5. We present a conclusion in Sec. 6. Proofs and additional theoretical developments are provided in Appendix A.

## 2. Solution of the Stochastic Inverse Problem

In developing the Bayesian solution of the SIP, we move from the most general formulation of the SIP to a practical formulation by layering the assumptions required for the development. The development is necessarily abstract because the intent is to establish the theoretical framework that provides the basis to compute a robustly accurate empirical approximation of a posterior distribution solving the eSIP that is conditioned on experimental data and the choice of prior.

### 2.1. Disintegration of measures

We consolidate the assumptions on the probability model for a random experiment.

**Assumption 2.1.**  $(\Lambda, \mathcal{B}_\Lambda)$  is a measurable space, where  $\Lambda \subset \mathbb{R}^n$ ,  $n \geq 1$ , is a bounded Borel measurable set and  $\mathcal{B}_\Lambda$  is the Borel  $\sigma$ -algebra restricted to  $\Lambda$ . We define  $Q : (\Lambda, \mathcal{B}_\Lambda) \rightarrow (\mathcal{D}, \mathcal{B}_\mathcal{D})$  as a random vector, where  $\mathcal{D} = Q(\Lambda) \subset \mathbb{R}^m$  for  $1 \leq m \leq n$  and  $\mathcal{B}_\mathcal{D}$  is the restriction of the Borel  $\sigma$ -algebra to  $\mathcal{D}$ .

The solution of the SIP is a posterior probability distribution that is conditioned on the observed data. To make this rigorous, we have to work within the framework of regular conditional probabilities conditioned on  $\sigma$ -algebras induced by random variables [4, 8, 21, 42],

[44, 59]. In this situation, we employ the fundamental tool for regular conditional probability measures called disintegration of measures.

**Remark 2.2.** A parallel development is found in geometric measure theory [29].

Disintegration provides a concrete way to express the fact that  $Q$  only provides information on a sub- $\sigma$ -algebra of  $\mathcal{B}_\Lambda$ , which restricts the possible inferences about  $P_\Lambda$  from observed data. Roughly speaking, disintegration is a way to express abstract statements involving conditional probabilities in terms of concrete integrals. In this sense, it serves the same purpose as Bayes' Theorem, though disintegration is more general.

The following result is an immediate consequence of the standard theory of disintegration [4, 8, 21, 42, 44, 59]. It is unfortunate that the result is rather impenetrable at first reading because it has profound practical implications for the use of conditional probability.

**Theorem 2.3.** *Assume that Assumption 2.1 holds and that  $\Psi_\Lambda$  is a bounded measure on  $(\Lambda, \mathcal{B}_\Lambda)$ . Let  $\Psi_{\mathcal{D}} = \Psi_\Lambda \circ Q^{-1}$  denote the induced measure on  $(\mathcal{D}, \mathcal{B}_{\mathcal{D}})$ . There is a family of probability measures  $\{\Psi_N(\cdot|q)\}_{q \in \mathcal{D}}$  on  $(\Lambda, \mathcal{B}_\Lambda)$  uniquely defined for  $\Psi_{\mathcal{D}}$ -almost every  $q \in \mathcal{D}$  such that*

$$\Psi_N(Q^{-1}(q)|q) = 1 \quad \text{and} \quad \Psi_N(\Lambda \setminus Q^{-1}(q)|q) = 0, \quad (2.1)$$

yielding the disintegration,

$$\Psi_\Lambda(A) = \int_{Q(A)} \Psi_N(A|q) d\Psi_{\mathcal{D}}(q) = \int_{Q(A)} \int_{Q^{-1}(q) \cap A} d\Psi_N(\lambda|q) d\Psi_{\mathcal{D}}(q) \quad (2.2)$$

for all  $A \in \mathcal{B}_\Lambda$ .

Note that while  $\Psi_N(\cdot|q)$  is a measure on  $\Lambda$ , it is nonzero only on the contour  $Q^{-1}(q)$ , which is a set of Lebesgue measure 0. We say that the  $\Psi_N(\cdot|q)$  is **concentrated** on  $Q^{-1}(q)$  and  $\Psi_\Lambda$  **disintegrates** to  $\{\Psi_N(\cdot|q)\}_{q \in \mathcal{D}}$  and  $\Psi_{\mathcal{D}}$ . Regular conditional probabilities conditioned on random variables and disintegration provide a systematic way to handle conditioning on sets of measure zero, and in particular, conditioning on observed data.

A common - but often unremarked - example of disintegration is the Product Measure Theorem [4] in which  $Q$  is the orthogonal projection onto some of the coordinates. (2.2) can be interpreted as a “nonlinear product measure theorem”, see Fig. 4. The inner integral  $\int_{Q^{-1}(q) \cap A} d\Psi_N(\lambda|q)$  gives the probability of the “slice” of  $A$  that intersects  $Q^{-1}(q)$ . We integrate these probabilities against the measure of the contours. The family  $\{\Psi_N(\cdot|q)\}_{q \in \mathcal{D}}$  consists of regular conditional probability measures  $\Psi_N(\cdot|q) = \Psi_N(\cdot|Q = q)$  conditioned on the data  $q$  [4]. Each  $\Psi_N(\cdot|q)$  is nonzero only on the generalized contour  $Q^{-1}(q)$ .

**Example 2.** We adapt a simple example from [4] that models observing the distance to the origin of a point chosen at random in a disk. Let  $\Lambda = \{(x_1, x_2) \in \mathbb{R}^2 : (x_1^2 + x_2^2)^{1/2} \leq 1\}$  and define  $Q : (\Omega, \mathcal{B}_\Lambda) \rightarrow ([0, 1], \mathcal{B}_{[0,1]})$  by  $Q(x_1, x_2) = (x_1^2 + x_2^2)^{1/2}$ . The generalized contours are circles of radius  $q$ . We assume that  $\Psi_\Lambda$  has density  $\rho_\Lambda$  with respect to the Lebesgue measure. Theorem 2.3 implies there is a family  $\{\Psi_N(\cdot|q)\}_{q \in [0,1]}$  concentrated on circles  $\{(x_1, x_2) : Q(x_1, x_2) = q, x_1, x_2 \in \mathbb{R}\}$  such that

$$\Psi_\Lambda(A) = \int_{[0,1]} \Psi_N(A|q) d\Psi_{\mathcal{D}}(q), \quad A \in \mathcal{B}_\Lambda.$$

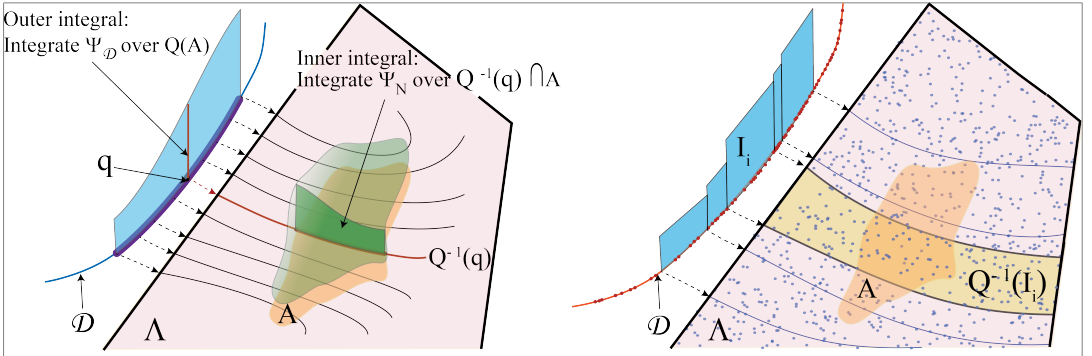


Fig 4. Left: we illustrate disintegration when the conditional probabilities are written in terms of densities. The probability on  $\Lambda$  is represented by a density shaded in green and the probability on  $\mathcal{D}$  is represented by a density shaded in blue. The disintegrated density on  $Q^{-1}(q)$  is indicated with a darker shade of green. Right: we illustrate the numerical solution method by random sampling. The observed data is indicated by dark red points on  $\mathcal{D}$  and the associated empirical distribution is shown in blue relative to the partition  $\{I_i\}$ . We show the samples  $\{\lambda_i\}$  in  $\Lambda$  as points and  $Q^{-1}(I_i)$  is shaded in gold. Figure is adapted from [47].

We identify the components of the integral on the right by a simple matching of terms. We first write an expression for the probability of an event  $A$  using polar coordinates,

$$\Psi_\Lambda(A) = \int_{[0,1] \times [0,2\pi]} \left( \chi_A(q, \theta) \rho_\Lambda(q \cos(\theta), q \sin(\theta)) \right) q \, d\mu_{\mathcal{L}}(\theta) \, d\mu_{\mathcal{L}}(q),$$

where  $\mu_{\mathcal{L}}$  denotes the Lebesgue measures on the appropriate sets and  $\chi_A$  denotes the **characteristic** or **indicator function** of  $A$ . We use Fubini's theorem<sup>1</sup> to write,

$$\begin{aligned} \Psi_\Lambda(A) &= \int_{[0,1]} \left( \frac{\int_{[0,2\pi]} \chi_A(q, \theta) \rho_\Lambda(q \cos(\theta), q \sin(\theta)) \, d\mu_{\mathcal{L}}(\theta)}{\int_{[0,2\pi]} \rho_\Lambda(q \cos(\theta), q \sin(\theta)) \, d\mu_{\mathcal{L}}(\theta)} \right) \\ &\quad \times \left( \int_{[0,2\pi]} \rho_\Lambda(q \cos(\theta), q \sin(\theta)) \, d\mu_{\mathcal{L}}(\theta) \right) q \, d\mu_{\mathcal{L}}(q), \end{aligned}$$

By identification, we recognize that,

$$d\Psi_{\mathcal{D}}(q) = \left( \int_{[0,2\pi]} \rho_\Lambda(q \cos(\theta), q \sin(\theta)) \, d\mu_{\mathcal{L}}(\theta) \right) q \, d\mu_{\mathcal{L}}(q).$$

and

$$\Psi_N(A|q) = \frac{\int_{[0,2\pi]} \chi_A(q, \theta) \rho_\Lambda(q \cos(\theta), q \sin(\theta)) \, d\mu_{\mathcal{L}}(\theta)}{\int_{[0,2\pi]} \rho_\Lambda(q \cos(\theta), q \sin(\theta)) \, d\mu_{\mathcal{L}}(\theta)},$$

which has conditional density,

$$\rho_N(\cdot|q) = \frac{\rho_\Lambda(q \cos(\theta), q \sin(\theta))(\theta)}{\int_{[0,2\pi]} \rho_\Lambda(q \cos(\theta), q \sin(\theta)) \, d\mu_{\mathcal{L}}(\theta)}. \quad (2.3)$$

<sup>1</sup>A simple consequence of disintegration.

## 2.2. Bayesian solution of the SIP

Theorem 2.3 implies that for any solution  $P_\Lambda$  of the SIP there is a family of probability measures  $\{P_N(\cdot|q)\}_{q \in \mathcal{D}}$  on  $(\Lambda, \mathcal{B}_\Lambda)$  uniquely defined  $P_\mathcal{D}$  a.e. such that

$$P_N(Q^{-1}(q)|q) = 1, \quad P_N(\Lambda \setminus Q^{-1}(q)|q) = 0, \quad (2.4)$$

and

$$P_\Lambda(A) = \int_{Q(A)} P_N(A|q) dP_\mathcal{D}(q) = \int_{Q(A)} \int_{Q^{-1}(q) \cap A} dP_N(\lambda|q) dP_\mathcal{D}(q) \quad (2.5)$$

for all  $A \in \mathcal{B}_\Lambda$ . Turning this around, any family  $\{P_N(\cdot|q)\}_{q \in \mathcal{D}}$  on  $(\Lambda, \mathcal{B}_\Lambda)$  satisfying (2.4) yields a solution of the SIP via (2.5). Of course, the data generating distribution  $P_\Lambda^d$  determines a unique a.e. family  $\{P_N^d(\cdot|q)\}_{q \in \mathcal{D}}$ , but this is unknown and cannot be determined by observations of the value of  $Q$ .

We are in a situation that is analogous to the use of Bayes' Theorem since neither the model nor the observed data give information about  $\{P_N(\cdot|q)\}_{q \in \mathcal{D}}$ . We adopt a Bayesian approach by describing prior information about the physical system in terms of a prior probability.

**Theorem 2.4.** *Assume that Assumption 2.1 holds. Assume that  $\{P_N(\cdot|q)\}_{q \in \mathcal{D}}$  is a family of probability measures on  $(\Lambda, \mathcal{B}_\Lambda)$  satisfying (2.4). There is a unique solution  $P_\Lambda$  of the SIP satisfying the disintegration (2.5).*

Theorem 2.4 establishes a **nonparametric Bayesian solution** of the SIP.  $\{P_N(\cdot|q)\}_{q \in \mathcal{D}}$  is called the **Ansatz prior** and it is (ideally) chosen based on prior belief and knowledge about the physical parameters in  $\Lambda$ . The solution  $P_\Lambda$  is a **posterior (probability distribution)** in an epistemological sense that represents the knowledge of encapsulated in the prior updated with the information provided by the observed data.

While specifying a family  $\{P_N(\cdot|q)\}_{q \in \mathcal{D}}$  offers the most general way to encapsulate prior knowledge in probabilistic terms, this is difficult in practice since generally we do not know the contours. Below we explain how to describe prior knowledge in terms of a more familiar **prior (distribution)**  $P_p$  on  $(\Lambda, \mathcal{B}_\Lambda)$  which yields an Ansatz prior family  $\{P_N(\cdot|q)\}_{q \in \mathcal{D}}$  implicitly.

**Example 3.** We present a discrete example adapted from [4, 22] that provides a simplistic but intuitive illustration of the Bayesian solution of the eSIP. We define the discrete probability space  $\Lambda = \{(\lambda_1, \lambda_2) \in \{1, 2, 3\} \times \{1, 2, 3\}\}$ , with the power set  $\sigma$ -algebra, and data generating probability measure,

$$P_\Lambda^d = \begin{bmatrix} 1/20 & 1/20 & 1/20 \\ 1/9 & 1/9 & 1/20 \\ 5/12 & 1/9 & 1/20 \end{bmatrix}.$$

Setting  $f(j) = \begin{cases} 0, & j \text{ odd}, \\ 1, & j \text{ even}, \end{cases}$ , we define  $Q(\lambda_1, \lambda_2) = f(\lambda_1 + \lambda_2)$ .  $Q : \Lambda \rightarrow \mathcal{D} = \{0, 1\}$ , so the generalized contours are,

$$Q^{-1}(0) = \{(1, 2), (2, 1), (2, 3), (3, 2)\}, \quad Q^{-1}(1) = \{(1, 1), (1, 3), (2, 2), (3, 1), (3, 3)\}.$$

The induced probability measure is  $\begin{pmatrix} P_{\mathcal{D}}(0) \\ P_{\mathcal{D}}(1) \end{pmatrix} = \begin{pmatrix} 29/90 \\ 61/90 \end{pmatrix} \approx \begin{pmatrix} .322 \\ .677 \end{pmatrix}$ . We now “forget”  $P_{\Lambda}^d$  and solve the eSIP conditioned on a choice of prior.

To obtain observational data for the eSIP, we compute 200 draws from a Bernoulli random variable with probability  $\frac{61}{90}$  of 1 and use these to compute the estimate  $\begin{pmatrix} \hat{P}_{\mathcal{D}}(0) \\ \hat{P}_{\mathcal{D}}(1) \end{pmatrix} = \begin{pmatrix} .34 \\ .66 \end{pmatrix}$ . We compute the solution of the eSIP corresponding to  $\hat{P}_{\mathcal{D}}$ . For reasons explained below, in the absence of prior information, we assume a uniform prior,

$$P_p = \begin{pmatrix} 1/9 & 1/9 & 1/9 \\ 1/9 & 1/9 & 1/9 \\ 1/9 & 1/9 & 1/9 \end{pmatrix}.$$

Since,  $\frac{\frac{1}{9}}{\frac{1}{9} + \frac{1}{9} + \frac{1}{9} + \frac{1}{9}} = \frac{1}{4}$  and  $\frac{\frac{1}{9}}{\frac{1}{9} + \frac{1}{9} + \frac{1}{9} + \frac{1}{9} + \frac{1}{9}} = \frac{1}{5}$ , we obtain the conditional distributions,

$$P_N(A|0) = \frac{1}{4}\chi_A(1, 2) + \frac{1}{4}\chi_A(2, 1) + \frac{1}{4}\chi_A(2, 3) + \frac{1}{4}\chi_A(3, 2),$$

$$P_N(A|1) = \frac{1}{5}\chi_A(1, 1) + \frac{1}{5}\chi_A(1, 3) + \frac{1}{5}\chi_A(2, 2) + \frac{1}{5}\chi_A(3, 1) + \frac{1}{5}\chi_A(3, 3),$$

where  $A$  is any set in  $\Lambda$  and  $\chi_A$  is the indicator function for set  $A$ , as well as the estimated solution of the eSIP,

$$\begin{aligned} \hat{P}_{\Lambda}(A) &= \left( \frac{1}{4}\chi_A(1, 2) + \frac{1}{4}\chi_A(2, 1) + \frac{1}{4}\chi_A(2, 3) + \frac{1}{4}\chi_A(3, 2) \right) .34 \\ &\quad + \left( \frac{1}{5}\chi_A(1, 1) + \frac{1}{5}\chi_A(1, 3) + \frac{1}{5}\chi_A(2, 2) + \frac{1}{5}\chi_A(3, 1) + \frac{1}{5}\chi_A(3, 3) \right) .66. \end{aligned} \quad (2.6)$$

(2.6) is a discrete version of the disintegration (2.5). If we have prior information that the points near  $(3, 1)$  are more likely, we might choose the prior,

$$\begin{pmatrix} 1/20 & 1/20 & 1/20 \\ 3/16 & 3/16 & 1/20 \\ 3/16 & 3/16 & 1/20 \end{pmatrix}, \quad (2.7)$$

yielding the estimate,

$$\begin{aligned} \hat{P}_{\Lambda}(A) &= \left( \frac{2}{19}\chi_A(1, 2) + \frac{15}{38}\chi_A(2, 1) + \frac{2}{19}\chi_A(2, 3) + \frac{15}{38}\chi_A(3, 2) \right) .34 \\ &\quad + \left( \frac{2}{21}\chi_A(1, 1) + \frac{2}{21}\chi_A(1, 3) + \frac{5}{14}\chi_A(2, 2) + \frac{5}{14}\chi_A(3, 1) + \frac{2}{21}\chi_A(3, 3) \right) .66, \end{aligned}$$

which indeed assigns higher probability to the points near  $(3, 1)$ .

### 2.3. The structural properties of $Q^{-1}$ .

In order to express the disintegration (2.5) in concrete terms, we develop the properties of  $Q^{-1}$ . In addition to Assumption 2.1, we assume the following holds.

**Assumption 2.5.**

1.  $\Lambda \subset \mathbb{R}^n$  is compact with measurable boundary  $\partial\Lambda$  satisfying  $\text{int}(\Lambda) = \Lambda$  and  $\mu_{\mathcal{L}}(\partial\Lambda) = 0$ , where  $\bar{B}$  is the closure of a set  $B$ ;
2. There is an open set  $U_{\Lambda}$  with  $U_{\Lambda} \supset \Lambda$  such that  $Q$  is continuously differentiable a.e. on  $U_{\Lambda}$ ;
3.  $Q$  is **geometrically distinct (GD)** on  $U_{\Lambda}$ , which means that the  $m \times n$  Jacobian matrix  $J_Q$  of  $Q$  is full rank  $m$  except on a finite union of manifolds of dimension less than or equal to  $n - 1$ .

The compactness of  $\Lambda$  is reasonable because parameters are generally bounded for most process models<sup>2</sup>. In fact, determining  $\Lambda$  is often an important part of constructing a model, see [47] where the choice of  $\Lambda$  for transmission rates for different strains of COVID-19 is discussed. Assuming  $\text{int}(\Lambda) = \Lambda$  and  $\mu_{\mathcal{L}}(\partial\Lambda) = 0$  are technical assumptions required for approximate solution by finite sampling. We illustrate in Fig. 5. The smoothness assumption on  $Q$  can be established for broad classes of models since it is typically assumed for numerical solution of the model. The assumption of GD means that  $\Lambda$  can be covered by a finite number of open sets up to a set of measure 0 such that  $J_Q$  has full rank  $m$  on each set. In these sets, no component of  $J_Q$  can be expressed as a linear combination of its other components. If this is violated,  $Q$  should be simplified to obtain a new  $Q$  map into a range with smaller dimension.

The important consequence of these assumptions is a concrete interpretation of generalized contours and the inner integral in (2.5).

**Theorem 2.6.** *Assume Assumptions 2.1 and 2.5 hold. For almost all  $q \in \mathcal{D}$ , the generalized contour  $Q^{-1}(q) = \{\lambda \in U_{\Lambda} \mid Q(\lambda) = q, \text{rank}(J_Q(\lambda)) = m\}$  is a  $n - m$ -dimensional a.e. smooth manifold immersed in  $\mathbb{R}^n$  and the inner integral in (2.5) is a surface integral defined for a piecewise smooth parameterization on  $(\mathbb{R}^{n-m}, \mathcal{B}_{\mathbb{R}^{n-m}}, \mu_{\mathcal{L}})$ .*

**Example 4.** Consider the integral (2.3) computed over circles using polar coordinates in Example 2.

We discuss the proof and recall some background information about manifolds in Sec. A.1. We reflect Theorem 2.6 by writing an integral of a conditional density  $f$  over a generalized contour  $Q^{-1}(q)$  as  $\int_{Q^{-1}(q) \cap A} f(s|q) ds$ , where  $s$  indicates the integral is computed for some suitable parameterization of  $Q^{-1}(q)$  over  $(\mathbb{R}^{n-m}, \mathcal{B}_{\mathbb{R}^{n-m}}, \mu_{\mathcal{L}})$ . In practice, we avoid computing such integrals in closed form, so the parameterization is immaterial.

## 2.4. Writing the solution of the SIP in terms of a conditional density

We develop a formula for the solution in terms of a conditional density function. We assume,

**Assumption 2.7.**  $P_{\mathcal{D}}$  is absolutely continuous with respect to  $\mu_{\mathcal{D}}$ , i.e.  $dP_{\mathcal{D}} = \rho_{\mathcal{D}} d\mu_{\mathcal{D}}$  a.e. for an integrable probability density function  $\rho_{\mathcal{D}}$ .

By Theorem 2.3, the Lebesgue measure disintegrates as,

$$\mu_{\Lambda}(A) = \int_{Q(A)} \mu_N(A|q) d\tilde{\mu}_{\mathcal{D}}(q) = \int_{Q(A)} \int_{Q^{-1}(q) \cap A} d\mu_N(\lambda|q) d\tilde{\mu}_{\mathcal{D}}(q), \quad (2.8)$$

<sup>2</sup>We emphasize that  $\Lambda$  is not the domain for parameters in a parameterized family of probability distributions.

where  $\{\mu_N(\cdot|q)\}_{q \in \mathcal{D}}$  is a family of regular conditional probability measures on  $(\Lambda, \mathcal{B}_\Lambda)$  such that  $\mu_N(\cdot|q)$  is concentrated on  $Q^{-1}(q)$  and  $\{\mu_N(\cdot|q)\}_{q \in \mathcal{D}}$  is unique  $\tilde{\mu}_{\mathcal{D}}$  a.e. with  $\tilde{\mu}_{\mathcal{D}} = Q\mu_\Lambda$ .

In light of (2.5) and (2.8), the relation between  $P_\Lambda$  and  $\mu_\Lambda$  depends on the relation between  $\{P_N(\cdot|q)\}_{q \in \mathcal{D}}$  and  $\{\mu_N(\cdot|q)\}_{q \in \mathcal{D}}$ . That relation can not be inferred from the model or the observed data. Instead, we specify an Ansatz prior. However, it is awkward and impractical to state a density result for a general Ansatz prior. Instead, we focus on the practical case of specifying a prior distribution  $P_p$  on  $(\Lambda, \mathcal{B}_\Lambda)$  with associated induced measure  $\tilde{P}_{p,\mathcal{D}} = QP_p$ . We assume,

**Assumption 2.8.** The prior  $P_p$  is absolutely continuous with respect to  $\mu_\Lambda$ , so  $dP_p = \rho_p d\mu_\Lambda$  for an integrable probability density  $\rho_p$  and  $\mu_N(\rho_p(\lambda) = 0|q) \neq 1$  for almost all  $q \in \mathcal{D}$ .

We have the main result, proved in § A.2.

**Theorem 2.9.** Assume Assumptions 2.1, 2.5, 2.7, and 2.8 hold. There is a solution of the SIP  $P_\Lambda$  that is absolutely continuous with respect to  $\mu_\Lambda$  and  $dP_\Lambda = \rho_\Lambda d\mu_\Lambda$  with

$$\rho_\Lambda(\lambda) = \frac{\rho_{\mathcal{D}}(Q(\lambda))}{\tilde{\rho}_{p,\mathcal{D}}(Q(\lambda))} \cdot \rho_p(\lambda) \quad \mu_\Lambda \text{ a.e.}, \quad (2.9)$$

where

$$\tilde{\rho}_{p,\mathcal{D}}(q) = \int_{Q^{-1}(q)} \rho_p \frac{1}{\sqrt{\det(J_Q J_Q^\top)}} ds.$$

Formula (2.9) is the nonparametric analog of the typical conclusion of Bayes' Theorem that is commonly used in Bayesian statistics.

## 2.5. The maximum entropy property of the uniform prior solution

The solution of the SIP corresponding to the **uniform prior**  $P_p = \frac{1}{\mu_\Lambda(\Lambda)}\mu_\Lambda$  has density,

$$\rho_\Lambda(\lambda) = \frac{\rho_{\mathcal{D}}(Q(\lambda))}{\tilde{\rho}_{\mathcal{D}}(Q(\lambda))} \quad \mu_\Lambda \text{ a.e.}, \quad \tilde{\rho}_{\mathcal{D}}(q) = \int_{Q^{-1}(q)} \frac{1}{\sqrt{\det(J_Q J_Q^\top)}} ds. \quad (2.10)$$

We call the solution corresponding to the uniform prior the **posterior solution conditioned on the uniform prior** or the **uniform prior (posterior) solution**.

The uniform prior has a special property that makes it the default choice for solving the SIP in the absence of an informed prior. Namely, it is an expression of the Principle of Insufficient Reason. The translation invariance of the uniform prior respects the fact that since distinct points on the generalized contour  $Q^{-1}(q)$  cannot be distinguished using data on  $Q$ , the probability of points on  $Q^{-1}(q)$  should be equal. The next theorem shows that the solution  $P_\Lambda$  corresponding to the uniform prior is the least biased solution of the SIP in a certain sense. We give the proof in § A.3.

**Theorem 2.10.** Assume Assumptions 2.1, 2.5, and 2.7 hold. The solution of the SIP corresponding to the uniform prior has maximum entropy among all solutions that are absolutely continuous with respect to  $\mu_\Lambda$  and whose prior is absolutely continuous with respect to the Lebesgue measure.

**Example 5.** In Example 3, the entropy of the SIP solution for the uniform prior is 2.1746 and the entropy for the solution for the prior (2.7) is 1.9805.

## 2.6. Continuity

We develop sufficient conditions that guarantee the density of the solution of the SIP is continuous a.e. A key ingredient is the a.e. continuity of the surface (Hausdorff) measure of the generalized contours. This depends on the interaction of the generalized contours with the boundary of  $\Lambda$ . For example, if the boundary has measure larger than 0, there is little chance that the surface measure of the contours is continuous, see Fig. 5.

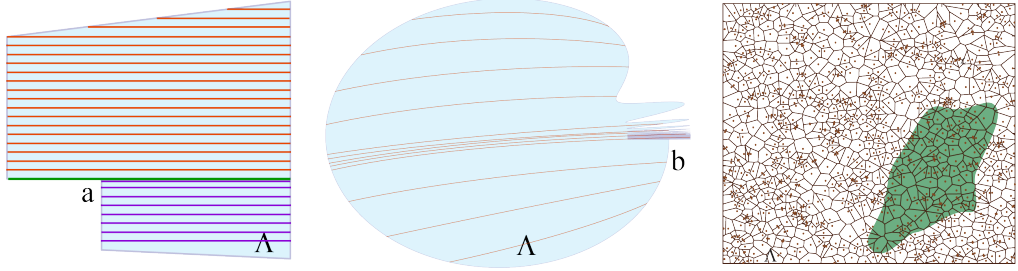


Fig 5. Left: generalized contour lines colored in red, green, and purple. The green contour line intersecting the boundary of  $\Lambda$  at the point  $a$  is parallel to the boundary and thus violates the rank condition on  $(J_Q \ J_B)^\top$ . The lengths of the contours obviously change discontinuously at the point  $a$ . Center: a domain whose boundary has Hausdorff measure larger than 1. The lengths of the contours that intersect the boundary in the complex area on the right change rapidly as contact point approaches the point  $b$ . Right: the Voronoi tessellation of the unit square for a sample from a uniform distribution.

To analyze the interaction of the generalized contours with the boundary of  $\Lambda$ , we assume the boundary is a piecewise smooth manifold. Specifically, we assume

**Assumption 2.11.**  $\partial\Lambda = \{\lambda : B(\lambda) = 0\}$  is determined by a continuously differentiable function  $B : U_\Lambda \rightarrow \mathbb{R}$  and, for  $q \in \mathcal{D}$  with  $\partial\Lambda \cap Q^{-1}(q) \neq \emptyset$ , the boundary  $Q^{-1}(q) \cap \partial\Lambda$  of  $Q^{-1}(q)$  in  $\Lambda$  is determined by the augmented system,

$$\begin{cases} Q(\lambda) - q = 0, \\ B(\lambda) = 0. \end{cases}$$

For all  $q \in \mathcal{D}$  with  $\partial\Lambda \cap Q^{-1}(q) \neq \emptyset$ ,  $(J_Q \ J_B)^\top$  is full rank on  $\partial\Lambda \cap Q^{-1}(q)$ .

The condition  $(J_Q \ J_B)^\top$  is full rank on  $\partial\Lambda \cap Q^{-1}(q)$  implies that the generalized contour is not tangent to the boundary at  $\partial\Lambda \cap Q^{-1}(q)$ , see Fig. 5.

The proof of the continuity result is given in § A.4.

**Theorem 2.12.** Assume Assumptions 2.1, 2.5, 2.7, 2.8, and 2.11 hold and the density of the prior  $\rho_p$  is continuous a.e. Then,  $\tilde{\rho}_{p,\mathcal{D}}(q)$  is continuous in a neighborhood of each point  $q \in \mathcal{D}$ . In addition, if the density function  $\rho_{\mathcal{D}}$  is continuous a.e., then the density  $\rho_\Lambda$  of the solution  $P_\Lambda$  corresponding to the prior  $P_p$  is continuous in a neighborhood of each point  $q \in \mathcal{D}$ .

We summarize the Bayesian solution of the SIP in classical inverse problem terms.

**Theorem 2.13.** Assume Assumptions 2.1, 2.5, 2.7, 2.8, and 2.11 hold and the densities  $\rho_p$  and  $\rho_{\mathcal{D}}$  are continuous a.e. The Bayesian solution of the SIP is well posed in the sense of Hadamard, i.e., it is unique and continuous a.e.

We emphasize that the assumptions for this result allow for wide-ranging practical application. Also, the result does not depend on regularization. Indeed, regularization would alter the sub- $\sigma$ -algebra induced by  $Q^{-1}$ , which is the information that the experiment provides about the parameters.

### 3. Numerical solution of the eSIP by reweighting random samples

In this section, we present and analyze a numerical solution method for the eSIP based on random sampling. The convergence analysis is conducted under the assumptions in Theorem 2.9 and the a.e. continuity of the solution is crucial.

#### 3.1. Properties of the random samples used for the estimate

We begin by describing the requirements on the random samples used to compute the estimate. We apply this material to both  $\Lambda$  and  $\mathcal{D}$ , so for the moment we consider a measurable set  $\Omega \subset \mathbb{R}^k$ ,  $k \geq 1$ , with measurable boundary of Lebesgue measure zero  $\mu_{\mathcal{L}}(\partial\Omega) = 0$  and Borel  $\sigma$ -algebra  $\mathcal{B}_{\Omega}$ . We let  $\mu_{\Omega}$  denote the Lebesgue measure restricted to  $\Omega$ .

A collection points  $\{\omega_j\}_{j=1}^M \subset \Omega$  defines a **Voronoi tessellation**  $\mathcal{V}_M = \{V_j\}_{j=1}^M$  that partitions  $\Omega$ , where  $V_j = \{\omega \in \Omega : d_v(\omega_j, \omega) \leq d_v(\omega_i, \omega), i = 1, \dots, M\}$ , for a specified metric  $d_v(\cdot, \cdot)$  on  $\Omega$ . For a set  $A \in \mathcal{B}_{\Omega}$  with  $\mu_{\Omega}(\partial A) = 0$ , the **Voronoi coverage** of  $A$  is defined  $A_M = \bigcup_{\omega_j \in A, 1 \leq j \leq M} V_j$ . We illustrate in Fig. 5.

A key property for approximation of sets by sequences of Voronoi tessellations is that the upper bound of the maximum inter-cell distance of cells in the sequence of Voronoi tessellations goes to zero a.s. Intuitively, this means the partitions  $\mathcal{V}_M$  becomes finer when  $M \rightarrow \infty$ . A rule for defining a sequence of samples  $\{\{\omega_j^{(\ell)}\}_{j=1}^{M_{\ell}}\}_{\ell=1}^{\infty}$  with associated Voronoi tessellations  $\{\mathcal{V}_{M_{\ell}}\}_{\ell=1}^{\infty}$ , where  $0 < M_1 < M_2 < \dots$ , is  $\mathcal{B}_{\Omega}$ -consistent if

$$r_{M_{\ell}} = \max_{1 \leq j \leq M_{\ell}} r(\omega_j^{(\ell)}) = \max_{1 \leq j \leq M_{\ell}} \max_{\omega \in V_j^{(\ell)}} d_v(\omega, \omega_j^{(\ell)}) \rightarrow 0 \text{ a.s. as } \ell \rightarrow \infty.$$

Generating collections of points by a Poisson point process that has an a.e. positive probability density function with respect to the Lebesgue measure is  $\mathcal{B}_{\Omega}$ -consistent, see Theorem A.4.

We assume,

**Assumption 3.1.** Collections of points  $\{\{d_i^{(\ell)}\}_{i=1}^{M_{\ell}}\}_{\ell=1}^{\infty}$  and associated Voronoi tessellations  $\{\mathcal{I}_{M_{\ell}}\}_{\ell=1}^{\infty}$  in  $\mathcal{D}$  and points  $\{\{\lambda_i^{(j)}\}_{i=1}^{N_j}\}_{j=1}^{\infty}$  and associated Voronoi tessellations  $\{\mathcal{T}_{N_j}\}_{j=1}^{\infty}$  in  $\Lambda$  are  $\mathcal{B}_{\mathcal{D}}$ -consistent resp.  $\mathcal{B}_{\Lambda}$ -consistent. Further, for sets  $C \in \mathcal{B}_{\mathcal{D}}$  with  $\mu_{\mathcal{D}}(\partial C) = 0$  and  $A \in \mathcal{B}_{\Lambda}$  with  $\mu_{\Lambda}(\partial A) = 0$ ,

$$\lim_{\ell \rightarrow \infty} \mu_{\mathcal{D}}(C_{M_{\ell}} \Delta C) = 0 \text{ a.s. and } \lim_{j \rightarrow \infty} \mu_{\Lambda}(A_{N_j} \Delta A) = 0 \text{ a.s.} \quad (3.1)$$

#### 3.2. Constructing the estimate

There are three discretizations involved with the eSIP; the number of observed data points  $K$ , the number of cells  $M$  in a partition of  $\mathcal{D}$ , and the number of cells  $N$  in a partition of  $\Lambda$ . However, limits on the accuracy of empirical density approximations means that  $M$  must be

related to  $K$ . We denote the observed data by  $\{q_i\}_{i=1}^\infty$ , which we assume is a random sample generated by a Poisson point process with distribution  $P_{\mathcal{D}}$ . For  $K \geq 1$ , we construct an approximation using  $\{q_i\}_{i=1}^K$  that is associated with a partition  $\mathcal{I}_{M_K}$  of  $\mathcal{D}$ , where the number of cells  $M_K$  in  $\mathcal{I}_{M_K}$  is a function of  $K$  that tends monotonically to  $\infty$  as  $K \rightarrow \infty$ . We assume the family  $\{\mathcal{I}_{M_K}\}_{K=1}^\infty$  satisfies Assumption 3.1. The approximation is also associated with partitions  $\{\mathcal{T}_{N_j}\}_{j=1}^\infty$  of  $\Lambda$ , which we assume satisfies Assumption 3.1.

To construct the approximation, we begin with a simple histogram estimate of  $\rho_{\mathcal{D}}$  on  $I_i$ ,

$$\hat{p}_{K,i} = \frac{\#q_k \in I_i^{(K)}}{K}, \quad 1 \leq i \leq M_K. \quad (3.2)$$

The approximation for  $P_\Lambda$  is

$$\hat{P}_{\Lambda,K,N_j}(A) = \sum_{i=1}^{M_K} \frac{\#\lambda_j^{(j)} \in A \cap Q^{-1}(I_i^{(K)})}{\#\lambda_j^{(j)} \in Q^{-1}(I_i^{(K)})} \hat{p}_{K,i}, \quad A \in \mathcal{B}_\Lambda. \quad (3.3)$$

We write the method in a form more conducive to analysis,

$$\hat{P}_{\Lambda,K,N_j}(A) = \sum_{i=1}^{M_K} \frac{\sum_{j=1}^{N_j} \chi_{\lambda_j^{(j)}}(Q^{-1}(I_i^{(K)}) \cap A)}{\sum_{j=1}^{N_j} \chi_{\lambda_j^{(j)}}(Q^{-1}(I_i^{(K)}))} \cdot \frac{1}{K} \sum_{k=1}^K \chi_{q_k}(I_i^{(K)}), \quad A \in \mathcal{B}_\Lambda. \quad (3.4)$$

This can be rewritten as

$$\hat{P}_{\Lambda,K,N_j}(A) = \sum_{i=1}^{M_K} \frac{\#\lambda_j^{(j)} \in A : Q(\lambda_j^{(j)}) \in I_i^{(K)}}{\#\lambda_j^{(j)} : Q(\lambda_j^{(j)}) \in I_i^{(K)}} \frac{\#q_k \in I_i^{(K)}}{K}, \quad A \in \mathcal{B}_\Lambda, \quad (3.5)$$

which shows that the estimate involves counting points in cells in the partition of  $\mathcal{D}$ .

An illustration of the method is presented in Fig. 4. Beginning with the observed data, we partition the range  $\mathcal{D}$  into a collection of cells and use the data to approximate the probability  $P_{\mathcal{D}}$  of each cell. The inverse image under  $Q$  of each cell in the partition of  $\mathcal{D}$  is a “fat” contour. As the cells in the partition of  $\mathcal{D}$  become smaller, the fat contours become “thinner”. We compute a sample of points in  $\Lambda$  distributed according to the prior. We estimate the probability of the intersection of a fixed set  $A$  with a fat contour by taking the ratio of the number of samples in the intersection of a fixed set  $A$  with the fat contour and the total number of samples in the fat contour. Finally, we sum up all the estimates over fat contours that intersect  $A$ , reweighting the estimate in each fat contour with the probability of its corresponding cell in  $\mathcal{D}$ . The key to convergence of this approach is the a.e. continuity of the surface measure of the contours. When a fat contour is sufficiently thin, the surface measures of almost all the contours in it are approximately the same.

### 3.3. The basic statistical properties of the estimate

These properties quantify how the estimate converges to the solution of the eSIP determined by the prior as all the discretizations are refined. We use the notation,

$$p_i^{(K)} = P_p(Q^{-1}(I_i^{(K)})) \quad \text{and} \quad \check{p}_i^{(K)} = P_p(A \cap Q^{-1}(I_i^{(K)})),$$

for all  $i$  and  $K$ . The ratio  $\frac{\check{p}_i^{(K)}}{p_i^{(K)}}$ , which features prominently, is the probability that a point selected at random on  $Q^{-1}(q)$  intersects  $A$ . We prove the theorem in § A.5.

**Theorem 3.2.** Assume Assumptions 2.1, 2.5, 2.7, 2.8, 2.11, and 3.1 hold and assume the densities  $\rho_p$  and  $\rho_{\mathcal{D}}$  are continuous a.e.

1. The estimate is asymptotically unbiased. For  $A \in \mathcal{B}_{\Lambda}$  with  $\mu_{\Lambda}(\partial A) = 0$ ,

$$E(\hat{P}_{\Lambda, K, N_j}(A)) = \sum_{i=1}^{M_K} \frac{\check{p}_i^{(K)}}{p_i^{(K)}} (1 - (1 - p_i^{(K)})^{N_j}) P_{\mathcal{D}}(I_i^{(K)}), \quad (3.6)$$

and  $\lim_{K \rightarrow \infty} \lim_{j \rightarrow \infty} E(\hat{P}_{\Lambda, K, N_j}(A)) = P_{\Lambda}(A)$ .

2. For  $A \in \mathcal{B}_{\Lambda}$  with  $\mu_{\Lambda}(\partial A) = 0$ ,

$$\lim_{j \rightarrow \infty} \text{Var}(\hat{P}_{\Lambda, K, N_j}(A)) \leq \frac{1}{K} \left( \sum_{i=1}^{M_K} P_{\mathcal{D}}(I_i^{(K)}) \frac{(\check{p}_i^{(K)})^2}{(p_i^{(K)})^2} - \left( \sum_{i=1}^{M_K} P_{\mathcal{D}}(I_i^{(K)}) \frac{\check{p}_i^{(K)}}{p_i^{(K)}} \right)^2 \right) \quad (3.7)$$

and  $\lim_{K \rightarrow \infty} \lim_{j \rightarrow \infty} \text{Var}(\hat{P}_{\Lambda, K, N_j}(A)) = 0$ .

3. The estimate is strongly consistent. For  $A \in \mathcal{B}_{\Lambda}$  with  $\mu_{\Lambda}(\partial A) = 0$ ,

$$\lim_{K \rightarrow \infty} \lim_{j \rightarrow \infty} \hat{P}_{\Lambda, K, N_j}(A) = P_{\Lambda}(A). \quad (3.8)$$

### 3.4. Asymptotic properties of the error of the estimate

We write,

$$\begin{aligned} \hat{P}_{\Lambda, K, N_j}(A) &= \sum_{i=1}^{M_K} \frac{\check{p}_i^{(K)}}{p_i^{(K)}} P_{\mathcal{D}}(I_i^{(K)}) + \sum_{i=1}^{M_K} \frac{\check{p}_i^{(K)}}{p_i^{(K)}} \left( \frac{1}{K} \sum_{k=1}^K \chi_{q_k}(I_i^{(K)}) - P_{\mathcal{D}}(I_i^{(K)}) \right) \\ &\quad + \sum_{i=1}^{M_K} \left( \frac{\sum_{j=1}^{N_j} \chi_{\lambda_j^{(K)}}(Q^{-1}(I_i^{(K)}) \cap A)}{\sum_{j=1}^{N_j} \chi_{\lambda_j^{(K)}}(Q^{-1}(I_i^{(K)}))} - \frac{\check{p}_i^{(K)}}{p_i^{(K)}} \right) \cdot \frac{1}{K} \sum_{k=1}^K \chi_{q_k}(I_i^{(K)}) \\ &= T_1 + T_2 + T_3. \end{aligned}$$

Since  $\lim_{K \rightarrow \infty} T_1 = P_{\Lambda}(A)$  a.e., we analyze the stochastic errors  $T_2$  and  $T_3$ .  $T_2$  depends on the error of the empirical approximations to  $P_{\mathcal{D}}(I_i^{(K)})$  while  $T_3$  depends on the empirical approximations to  $\check{p}_i^{(K)} / p_i^{(K)}$ .

For  $T_2$ , we prove the following in § A.6.

**Theorem 3.3.** Assume Assumptions 2.1, 2.5, 2.7, 2.8, 2.11, and 3.1 hold and assume the densities  $\rho_p$  and  $\rho_{\mathcal{D}}$  are continuous a.e.. Then,  $\lim_{K \rightarrow \infty} \sqrt{K} T_2 \stackrel{d}{=} \mathcal{N}(0, \sigma_p^2)$ , where

$$\sigma_p^2 = \int P_{p, N}(A|q)^2 dP_{\mathcal{D}}(q) - \left( \int P_{p, N}(A|q) dP_{\mathcal{D}}(q) \right)^2. \quad (3.9)$$

The second moment  $\sigma_p^2$  quantifies the variation in the disintegrated conditional probabilities conditioned on the data as the observations vary. We can control  $T_2$  by increasing the amount of observed data.

Obtaining a simple asymptotic result for  $T_3$  is apparently more difficult. We summarize the analysis presented in § A.6. The size of  $T_3$  is determined by the expressions,

$$T_{3, i, j} = \frac{\sum_{j=1}^{N_j} \chi_{\lambda_j^{(K)}}(Q^{-1}(I_i^{(K)}) \cap A)}{\sum_{j=1}^{N_j} \chi_{\lambda_j^{(K)}}(Q^{-1}(I_i^{(K)}))} - \frac{\check{p}_i^{(K)}}{p_i^{(K)}}, \quad 1 \leq i \leq M_K, 1 \leq j.$$

We prove,

**Theorem 3.4.** *Assume Assumptions 2.1, 2.5, 2.7, 2.8, 2.11, and 3.1 hold and assume the densities  $\rho_p$  and  $\rho_{\mathcal{D}}$  are continuous a.e. Then,  $\lim_{J \rightarrow \infty} E(T_{3,i,J}) = 0$  and  $\lim_{J \rightarrow \infty} \text{Var}(T_{3,i,J}) = 0$ .*

Roughly speaking, the proofs in § A.6 imply that to make  $T_3$  small,  $N_J p_i^{(K)}$  has to be large for all  $i$ . As  $K \rightarrow \infty$ ,  $Q^{-1}(I_i^{(K)})$  become “narrower” and  $p_i^{(K)} \downarrow 0$ .  $N_J$  has to increase at least linearly with  $1/p_i^{(K)}$  to ensure  $T_3$  becomes small.

### 3.5. Using other estimators of $\rho_{\mathcal{D}}$

We consider a general estimate  $\hat{\rho}_{k,i} = \hat{P}_{\mathcal{D}}(I_i^{(k)})$  in (3.3), where  $\hat{P}_{\mathcal{D}}$  has density  $\hat{\rho}_{\mathcal{D}}$  with respect to  $\mu_{\mathcal{D}}$ . We prove the following theorem in § A.7.

**Theorem 3.5.** *Assume Assumptions 2.1, 2.5, 2.7, 2.8, 2.11, and 3.1 hold and assume the densities  $\rho_p$  and  $\rho_{\mathcal{D}}$  are continuous a.e. If  $\hat{\rho}_{\mathcal{D}} \xrightarrow{L^1} \rho_{\mathcal{D}}$   $P_{\mathcal{D}}$  a.e., then  $\hat{P}_{\Lambda,K,N_J}$  is strongly consistent and (3.8) holds.*

We apply this theorem to a kernel density estimate (KDE). Choosing a **kernel function**  $\Xi$  (measurable, nonnegative, and  $\int \Xi d\mu_{\mathcal{D}} = 1$ ), we define

$$\hat{\rho}_{\mathcal{D}}(q) = \frac{1}{Kh_K^m} \sum_{i=1}^K \Xi\left(\frac{q - q_i}{h_K}\right),$$

where  $h_K$  is a **scaling length**. Theorem 6.1 of [25] implies that if

$$\lim_{K \rightarrow \infty} h_K + (Kh_K^m)^{-1} = 0, \quad (3.10)$$

then  $\int_{\mathcal{D}} |\hat{\rho}_{\mathcal{D}} - \rho_{\mathcal{D}}| d\mu_{\mathcal{D}} \rightarrow 0$  and Theorem 3.5 holds.

On another hand, if  $\rho_{\mathcal{D}}$  belongs to a parameterized family of distributions  $P_{\mathcal{D}}(q : \theta)$  with parameters  $\theta \in \Theta$ , we define the estimate  $\hat{\rho}_{\mathcal{D}}(q) = \rho_{\mathcal{D}}(q : \hat{\theta})$  for parameter estimate  $\hat{\theta}$ . To use Theorem 3.5, we require family of distributions and an estimate  $\hat{\theta}_K$  computed from data  $\{q_i\}_{i=1}^K$  such that  $\hat{\rho}_{\mathcal{D}}(\cdot : \hat{\theta}_K) \xrightarrow{L^1} \rho_{\mathcal{D}}(\cdot : \theta)$   $P_{\mathcal{D}}$  a.e. as  $\lim_{K \rightarrow \infty} \hat{\theta}_K = \theta$ . For example, the Beta distribution with a maximum likelihood estimate satisfies this condition.

## 4. Examples

We present a couple of simple examples that illustrate the results above. Applications of the eSIP to more complex models with higher dimensional parameter spaces can be found in [6, 10, 12, 13, 14, 15, 16, 18, 36, 43, 47, 53, 54]. The numerical solutions of the eSIP problems in the following examples are computed using the open-source software BET [37].

**Example 6.** We present visual evidence regarding convergence using Example 1. We hold the discretization and computational parameters fixed as in Example 1 except as noted. In the first experiment, we vary the number of points  $N_J \in \{50^2, 100^2, 400^2, 1600^2\}$  in the samples  $\{\lambda_i\}_{i=1}^{N_J}$  used to partition  $\Lambda$ . We plot the results in Fig. 6. There are visible resolution issues in the heatmap when  $N_J = 50^2$ . The increasing resolution is apparent up to  $N_J = 1000^2$  but

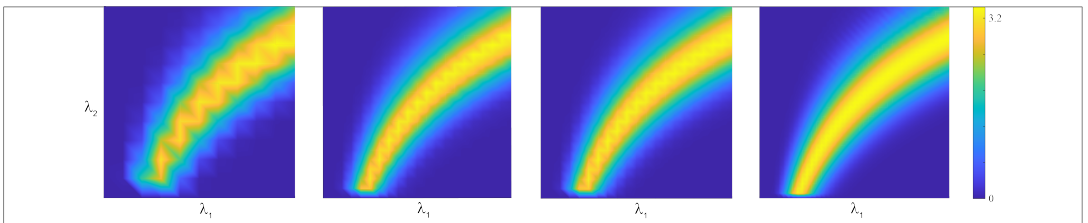


Fig 6. Heatmaps of solutions of the uniform prior SIP solution for the exponential decay model for  $T = 2$  computed using tessellation points  $\{\lambda_i\}_{i=1}^{N_J} \in \Lambda$  for  $N_J \in \{50^2, 100^2, 400^2, 1600^2\}$  in order from left to right.

there is little improvement after that. In the second experiment, we vary the number of cells  $M_K \in \{12, 25, 50, 100, 200\}$  in the partition  $\{I_i\}_{i=1}^{M_K}$  of  $\mathcal{D}$ . We plot the results in Fig. 7. The lower values of  $M_k$  result in poor resolution of  $P_{\mathcal{D}}$  because the “fat” contours are too fat. The increasing resolution is apparent up to  $M_K = 100$  but there is little improvement after that. The results shown in the lefthand plots in Fig.s 6 and 7 illustrate the analysis that requires

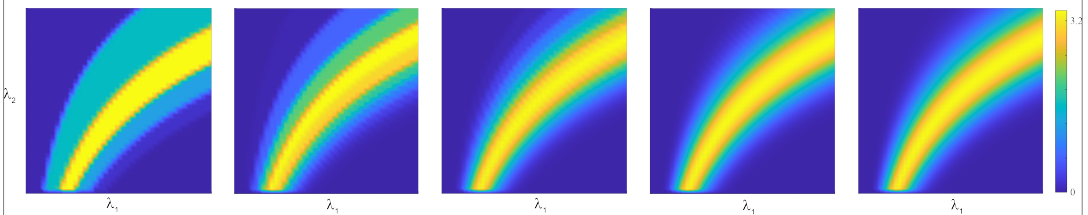


Fig 7. Heatmaps of solutions of the uniform prior SIP solution for the exponential decay model for  $T = 2$  computed using partitions  $\{I_i\}_{i=1}^{M_K}$  of  $\mathcal{D}$  for  $M_K \in \{12, 25, 50, 100, 200\}$  in order from left to right.

$M_K$  and  $N_J$  to become large together in order to improve accuracy.

**Example 7.** We solve the eSIP for parameters in a real-world experiment involving falling objects. While the example is simple, it presents challenges involved with formulating and solving an eSIP that generally arise in any application.

**The experiment.** The **standard acceleration of gravity**  $g$  is a model quantity approximating the acceleration experienced by an object falling near the surface of a planet. It is derived from the equation for the force of gravity on the object assuming that the distance of the object from the center of mass of the planet can be considered roughly constant while the object is falling. For a falling object near the surface of the earth,  $g \approx 9.81$ . However, since the earth is not a perfect sphere, the value of  $g$  depends on the location and varies by as much as .5%. In June 2013, author Bingham and our colleague Dave Higdon performed an experiment with the aim of determining the value of  $g$  in Vancouver British Columbia.

**The experimental set up and observed data.** They dropped a golf ball, tennis ball, baseball, volleyball and bowling ball<sup>3</sup> from a spot on the Alex Fraser Bridge approximately 35m above the ground, which lies approximately at sea level. The balls were launched horizontally to have a clear flight path, see Fig. 8. Relevant physical parameters of the balls obtained

<sup>3</sup>The collection also included a wiffle ball, but the physical parameters of those are very different from the others so we exclude that data.

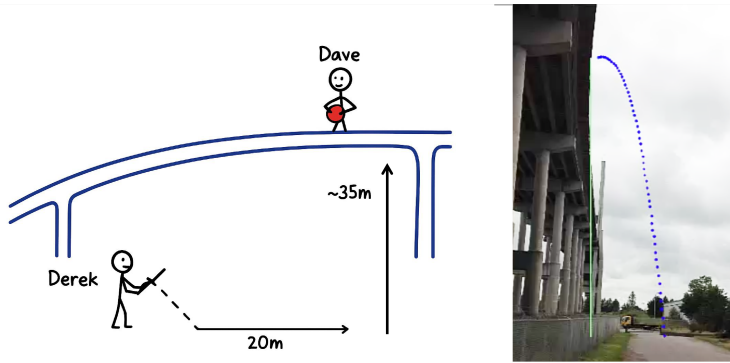


Fig 8. Left: Illustration of the ball dropping experiment. Right: A frame from a video capture of a trial.

from [55] are listed in Table 1. Additionally, the temperature was about 65°F. Each ball was

type	mass	diameter	Coefficient of Drag ( $C_d$ )	Terminal Velocity
golf ball	46g	42.7mm	.45	25 m/s
tennis ball	57g	65mm	.6	20 m/s
baseball	142g	70.8mm	.3	40 m/s
volleyball	260g	210mm	.12-.54	15.9 m/s
basketball	591g	240mm	.54	20.2 m/s
bowling ball	7.26kg	218mm	.47	83.1 m/s

Table 1

Physical parameters of the balls in the experiment [55].

dropped 2-5 times. The motion was captured by video and the time of flight was computed using *Logger Pro* software. The 17 measured times in seconds are given in Table 2. The low number of data points is a consequence of the intervention of the local authorities during the experiment.

	baseball	basketball	volleyball	bowling ball	golf ball	tennis ball
	2.8367	2.9033	2.6033	2.7383	2.7700	3.0367
	2.8383	3.0050	3.0700	2.7717	2.8367	3.0717
		2.8383	3.1383	2.7367		
		2.9033				
		2.8700				
average	2.8375	2.9040	2.9372	2.7489	2.8034	3.0542

Table 2

Flight times in seconds of the balls in the experiment. Last row shows averages.

**Choosing the model.** If the flight time of a falling object is sufficiently long, the effects of air resistance cannot be ignored. Generally, the velocity of a falling object grows more or less linearly at first, but the velocity eventually levels off to reach a constant **terminal velocity**. Taking into account the effects of air resistance, a high fidelity model is

$$\frac{dv}{dt} = -g + \frac{1}{2} \rho C_d \frac{A}{m} v^2, \quad (4.1)$$

where  $v$  is the *vertical velocity* of the following object,  $g$  is the *gravitational constant*,  $\rho$  is the *air density*,  $C_d$  is the *coefficient of drag*,  $m$  is the *mass*, and  $A$  is the *cross-sectional area*. The second term on the right, which is the nonnegative *drag term*, models the effect of air resistance. Since it scales with velocity squared, it is negligible for small velocity.

The model (4.1) is accompanied by an *initial height* of release  $H_0$  and *initial vertical velocity*  $V_0$ . In the dropping ball experiment, both  $H_0$  and  $V_0$  are uncertain because they vary with each trial. The QoI is the time of flight  $T$ .

There is a closed form solution of the model (4.1), though it is complicated to evaluate. However, using the full model (4.1) has some drawbacks. If we treat  $g$ ,  $\rho$ ,  $C_d$ ,  $A$ ,  $m$ ,  $H_0$ , and  $V_0$  as uncertain parameters, then we are solving an SIP for a distribution on a seven dimensional parameter space from a one dimensional observation. Since the prior disintegrates to a uniform distribution on the six dimensional generalized contours, the eSIP solution will have significant indeterminacy. Alternatively, since  $\rho$ ,  $C_d$ ,  $m$ , and  $A$  can be measured independently, we could treat them as random effects. However, if we substitute values from Table 1 into (4.1), we obtain a different model for each type of ball. This means we only have 2-5 samples for the eSIP for each type of ball. Moreover, we would have to deal with the complexity of the constrained eSIP [5].

Given these complications, it is reasonable to ask if including the drag term in the model (4.1) is important. While the terminal velocities of the balls vary significantly, wind tunnel data indicates that none of them are close to terminal velocity in the  $\approx 3$  seconds of the drops and their velocities remain well within the linear growth regime that is relevant when the drag force is negligible [55]. Indeed, the estimated differences in falling times between neglecting and including the effects of drag force are on the order of 2% – 3% for the time of flight. Thus, we reduce to a simpler model that neglects drag force,

$$\frac{dv}{dt} = -g, \quad (4.2)$$

with solution  $H(t) = -\frac{1}{2}gt^2 + V_0t + H_0$ ,  $t \geq 0$ , where  $H(t)$  is the height at time  $t$ . Solving for the QoI impact time gives  $T = \frac{1}{g}(V_0 + \sqrt{V_0^2 + 2gH_0})$ . Neglecting the drag force, means that we solve a single eSIP for all of the balls collectively so we have 17 data points. The cost is that the nominal uncertainty of all three parameters is increased because the potential effects of drag must be accommodated in some way.

With  $(H_0 \ V_0 \ g)^\top$  as the set of parameters for the eSIP for the simple model, we choose  $\Lambda = [27, 43] \times [-1, 1] \times [8.8, 10.8]$  centered on the nominal values  $(35 \ 0 \ 9.8)^\top$ . This allows a large degree of uncertainty in the parameters.

**Dealing with a small amount of data.** The number of observations ( $N_J = 17$ ) is too small to accurately estimate  $\hat{p}_{K, M_K, i}$  directly. We illustrate how to deal with this using simulation-based inference on the distribution of the experimental data by describing two approaches. First, we use a Beta distribution fitted to the observations to generate synthetic data for solving the eSIP. Alternatively, we augment the measured values by adding i.i.d. noise to produce a sufficiently large dataset for the eSIP. This approach amounts to jittering the observations many times to create a smoother empirical distribution function. We use this noisy data to solve the eSIP.

Allowing for additional uncertainty beyond the minimum and maximum values of the data in Table 2, we define the interval  $\mathcal{D} = [2.55, 3.19]$  in the measured units of time.

For the first approach, we use maximum likelihood to fit the Beta distribution to the data obtained by shifting the midpoint of  $\mathcal{D}$  to 1/2 then scaling the resulting set to  $[0, 1]$ . The estimated distribution on the unit interval is Beta(2.191, 2.047). We reverse the transformation to obtain a shifted and scaled Beta distribution on  $\mathcal{D}$ . Finally,  $10^6$  random samples are generated from this distribution to use for solving the eSIP.

In the second approach, we create a set of “noisy” output data by simulating 50,000 iid samples from the Beta(8, 8) distribution shifted and scaled to the interval  $[q_i - .35, q_i + .35]$  for each  $q_i$  value in Table 2 ( $17 \times 50,000$  is on the order of  $10^6$ ). We use equal parameters in the Beta distribution so the noise is symmetric.

For both approaches, we use  $N = 27 \times 10^6$  samples in  $\Lambda$  and  $M = 80$  partitions of  $\mathcal{D}$  to compute the solution of the eSIP for the uniform prior. We use a large numbers of samples for the discretization to reduce inaccuracies arising from finite Monte Carlo sampling. We obtain qualitatively similar results using samples on the order of hundreds.

**Solving the eSIP.** We show the eSIP solution corresponding to fitting a Beta distribution to the observed data in Fig. 9. The solution locates a region of highest relative probability near the corner  $(43 \ 1 \ 8.8)^\top$ , which is largest permissible height and upwards velocity and lowest permissible value for the gravitational constant. Values in this region increase the time of fall, and presumably are compensating for elimination of the effects of drag in the simple model.

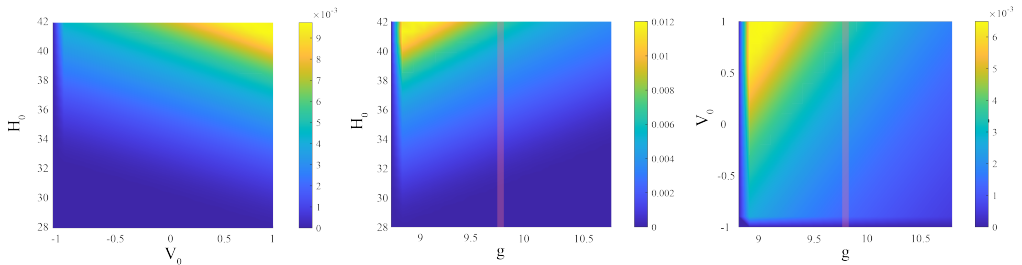


Fig 9. Heatmaps of marginal distributions for the solution of the eSIP computed using a parametric fit to the observed data. Left:  $H_0$  vs  $V_0$ . Center:  $H_0$  vs  $g$ . Right:  $V_0$  vs  $g$ . We indicate the part of  $\Lambda$  intersecting the realistic range of uncertainty for  $g$  near sea level as a transparent vertical rectangle in the second and third plots.

We show the eSIP solution corresponding to creating “noisy” output data in Fig. 10. This solution also places the highest probability near the corner point  $(43 \ 1 \ 8.8)^\top$ .

**Remark 4.1.** The effective support of the distribution is much smaller than that of the solution computed from fitting the data with a Beta distribution. Further testing shows that decreasing the range of the noise to  $[q_i - .2, q_i + .2]$  for each  $q_i$  produces a solution that very closely resembles the solution obtained with fitted data.

**The effect of removing outliers in the data.** The eSIP solutions in Figures 9 and 10 give cause for concern. Realistically, the variation in the gravitational constant near sea level is on the order of  $\pm 0.02 \text{ m/s}^2$ . Looking at the solution to the eSIP, we see that values within  $g \in [9.78, 9.82]$  have relatively low probability for either solution.

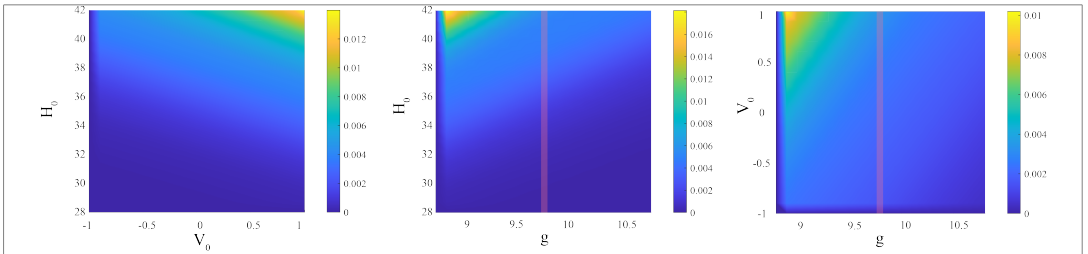


Fig 10. Heatmaps of marginal distributions for the solution of the eSIP computed using noisy data. Left:  $H_0$  vs  $V_0$ . Center:  $H_0$  vs  $g$ . Right:  $V_0$  vs  $g$ . We indicate the part of  $\Lambda$  intersecting the realistic range of uncertainty for  $g$  near sea level as a transparent vertical rectangle in the second and third plots.

One possible reason is that neglecting drag for some of the balls may be unrealistic. We note that the fall times of the volleyball and the tennis ball are generally larger than the other types of balls. If we fix  $H_0 = 35$  and  $V_0 = 0$  and use the crude estimate  $g \approx 2H_0/T^2$ , the volleyball and the tennis ball give significantly lower estimates than the other balls. We repeat the computations after removing the data for the volleyball and the tennis ball.

Fitting a Beta distribution to the data yields Beta(1.394, 2.030) (on the unit interval). We generate  $10^6$  random samples from this distribution to use for solving the eSIP. We use  $N = 27 \times 10^6$  samples in  $\Lambda$  and  $M = 80$  partitions of  $\mathcal{D}$  to compute the solution for the uniform prior, see Fig. 11.

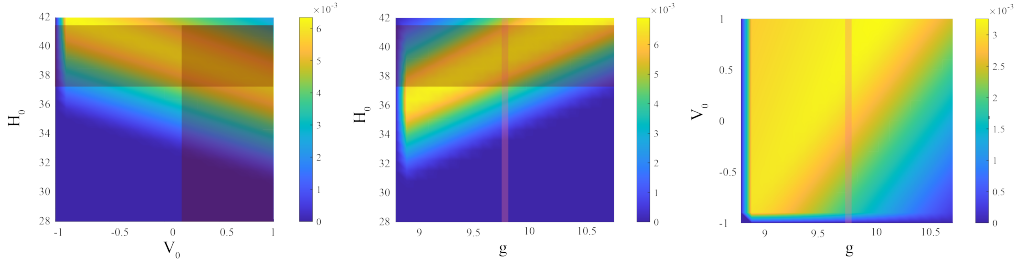


Fig 11. Heatmaps of marginal distributions for the solution of the eSIP computed using a parametric fit to observed data obtained by dropping volleyball and tennis ball data. Left:  $H_0$  vs  $V_0$ . Center:  $H_0$  vs  $g$ . Right:  $V_0$  vs  $g$ . We indicate the part of  $\Lambda$  intersecting the realistic range of uncertainty for  $g$  near sea level as a transparent vertical rectangle in the second and third plots. In the first and second plots, we indicate the intersection of  $\Lambda$  with the highly probable range of  $H_0$  given the realistic range of  $g$  as a transparent horizontal rectangle. In the first plot, we indicate the intersection of  $\Lambda$  with the highly probable range of  $V_0$  as a transparent vertical rectangle.

Next, we generate “noisy” output data by adding 70,000 iid samples from the Beta(8, 8) distribution scaled and shifted to  $[q_i - .35, q_i + .35]$  for each  $q_i$  value, excepting the volleyball and tennis ball data, in Table 2. The other computational parameters remain the same. We show the solution in Fig. 12. Interestingly, the eSIP solutions for the two different approaches to generating data are qualitatively similar.

The solutions obtained by eliminating the data for the volleyball and the tennis ball are quite different than the solutions obtained for the full set of data. Notably, the structure in the densities imparted from the linear contours combined with the uniform prior is evident. A

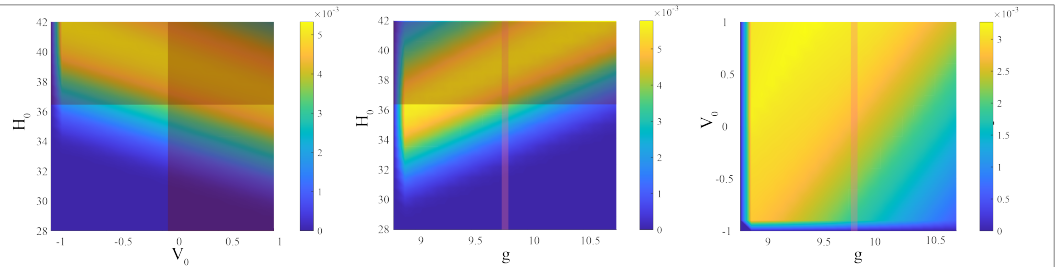


Fig 12. Heatmaps of marginal distributions for the solution of the eSIP computed using noisy data. Left:  $H_0$  vs  $V_0$ . Center:  $H_0$  vs  $g$ . Right:  $V_0$  vs  $g$ . We indicate the part of  $\Lambda$  intersecting the realistic range of uncertainty for  $g$  near sea level as a transparent vertical rectangle in the second and third plots. In the first and second plots, we indicate the intersection of  $\Lambda$  with the highly probable range of  $H_0$  given the realistic range of  $g$  as a transparent horizontal rectangle. In the first plot, we indicate the intersection of  $\Lambda$  with the highly probable range of  $V_0$  as a transparent vertical rectangle.

much larger set of possible parameter values produce solutions consistent with the observed data with relatively high probability.

In particular, there is a large range of  $H_0$  and  $V_0$  values that are consistent with  $g$  close to 9.8. We plot the event for  $g \in [9.78, 9.82]$  in Fig. 11 and 12 as vertical rectangles. Using the intersection of that event with the region of relatively high probability determines ranges for  $H_0$  of [37.5, 42.5] respectively [36.75, 43] of relatively high probability. Lastly, this indicates that  $V_0$  is in the range of [0, 1]. We also see that the region of relatively high probability has the property that larger values of  $H_0$  are associated with more negative values of  $V_0$  and vice versa, which fits intuition.

**Solving the eSIP for the bowling ball data with an informed prior.** Since the drag term in (4.1) is inversely proportional to the mass of the falling object, it appears that the flight of the bowling ball might best be described by the simple model (4.2) so we solve the eSIP using only the bowling ball data. Since we only have three data points, we use the noisy data approach to generate data for the eSIP with a much smaller range for the noise. We use a Beta distribution shifted and scaled to  $[q_i - .03, q_i + .03]$  for each data point. We also choose an “informed” prior. Since we are dealing with a single type of ball, it is reasonable to believe that there is less variation in the experimental uncertainty in  $H_0$  and  $V_0$  during the trials. We also estimate those uncertainties to within a physically realistic level. Finally, we restrict the uncertainty in  $g$  to a realistic level given we have strong prior knowledge about its value. We choose a normal prior with independent marginals  $N(35, .1)$  for  $H_0$ ,  $N(0, .1)$  for  $V_0$ , and  $N(9.81, .01)$  for  $g$ . We use the same sample space as above since we do not know the uncertainty introduced by dropping the drag term. We use  $2 \times 10^7$  samples to generate the sample from the prior and fix all of the other computational parameters as above.

We show the solution in Fig. 13. The effect of using a prior with a small effective support is obvious as the solution is also concentrated in a small region. The mode of the solution is near  $(35.7, 9.9)^T$  and the event of relatively high probability places  $g$  within  $[9.78, 9.95]$ .

**Remark 4.2.** Very similar results are obtained for a variety of small variances in the normal prior.

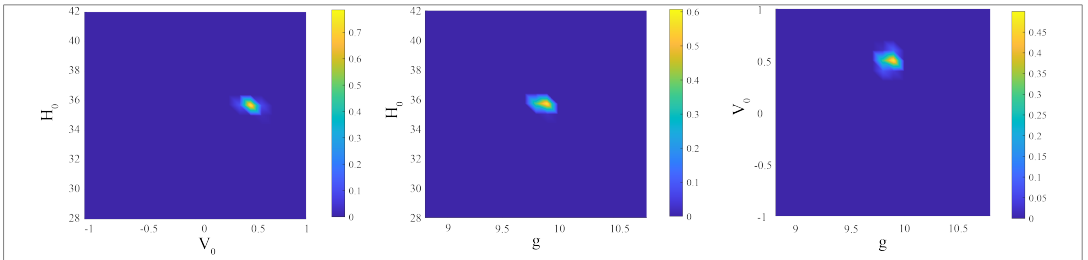


Fig 13. Heatmaps of marginal distributions for the solution of the eSIP computed using noisy data for the bowling ball and an informed prior. Left:  $H_0$  vs  $V_0$ . Center:  $H_0$  vs  $g$ . Right:  $V_0$  vs  $g$ .

**Conclusions.** The main conclusion is that the experimental uncertainty, the uncertainty introduced into the parameters in the simple model as a result of neglecting drag force, and the small amount of data means that we cannot determine more than two digits of accuracy for  $g$  from this experiment and model.

Including the volleyball and tennis ball data in the eSIP for the simplified model results in solutions that compensate for neglecting drag by putting higher probability on combinations of the parameters that produce longer drop times. Eliminating those data results in a solution that more accurately reflects the structure imparted by the model. Using an informed prior for the eSIP with the bowling ball data lead to a solution that is locally concentrated near a point, but did not yield a more accurate estimate.

## 5. An accept-reject solution method for the eSIP

As a partial connection to Markov Chain Monte Carlo methods typically used for Bayesian statistics, we adapt an accept-reject algorithm from [16] to construct a method for the eSIP that produces a collection of independent random samples approximately distributed according to the posterior distribution. The accept-reject criteria is based on the “update” weight,

$$\frac{\rho_{\mathcal{D}}(Q(\lambda))}{\tilde{\rho}_{p,\mathcal{D}}(Q(\lambda))},$$

applied to the prior density  $\rho_p(\lambda)$  in (2.9). We use the same setup as for the random sampling method presented in § 3, but simplify notation. The algorithm uses the estimate computed from the observed data,

$$\hat{\rho}_{\mathcal{D}}(Q(\lambda)) = \sum_{i=1}^M \left( \frac{1}{K} \sum_{k=1}^K \chi_{q_k}(I_i) \right) \chi_{I_i}(Q(\lambda)),$$

on a partition  $\{I_i\}_{i=1}^M$  of  $\mathcal{D}$  from a family satisfying Assumption 3.1. The algorithm also uses the estimate,

$$\tilde{\rho}_{p,\mathcal{D}}(Q(\lambda)) = \sum_{i=1}^M \left( \frac{1}{N} \sum_{k=1}^N \chi_{\lambda_k}(I_i) \right) \chi_{I_i}(Q(\lambda)),$$

computed from independent samples  $\{\lambda_k\}_{k=1}^N \in \Lambda$  distributed according to  $P_p$ . The accept-reject algorithm is,

**Algorithm 1:** Accept-Reject Algorithm for the eSIP

```

1 begin
2   Initialization:
3   Generate independent samples  $\{\lambda_i\}_{i=1}^N \in \Lambda$  distributed according to  $P_p$  and compute  $\{Q(\lambda_i)\}_{i=1}^N$ 
4   Construct  $\hat{\rho}_{\mathcal{D}}$  and  $\tilde{\rho}_{p,\mathcal{D}}$  and set  $C = \max \frac{\hat{\rho}_{\mathcal{D}}}{\tilde{\rho}_{p,\mathcal{D}}}$ .
5   for  $k = 1$  to  $N$  do
6     Generate a random sample  $\xi$  from the uniform distribution on  $[0, 1]$ 
7     if  $\xi > \frac{\hat{\rho}_{\mathcal{D}}(Q(\lambda_k))}{\tilde{\rho}_{p,\mathcal{D}}(Q(\lambda_k))C}$  then
8       remove  $\lambda_k$  from the collection
9   return Independent samples  $\{\check{\lambda}_k\}_{k=1}^{\check{N}} \subset \{\lambda_i\}_{i=1}^N$ 

```

The samples  $\{\check{\lambda}_k\}_{k=1}^{\check{N}}$  are approximately distributed according to the SIP solution distribution  $P_{\Lambda}$  with density,

$$\rho_{\Lambda}(\lambda) = \frac{\rho_{\mathcal{D}}(Q(\lambda))}{\tilde{\rho}_{p,\mathcal{D}}(Q(\lambda))} \cdot \rho_p(\lambda).$$

In our experience, the solution method based on reweighting random samples is generally more computationally efficient, especially if there is a high reject rate in the accept-reject method.

**Example 8.** We apply the accept-reject algorithm 1 to solve the eSIP in Example 1 using synthetic data. We hold the discretization and computational parameters fixed as in Example 1 except as noted. We choose  $K = 100$  for a uniform partition of  $\mathcal{D} = [0, 1]$ . We use  $N = 10^6$  samples from the data generating distribution  $P_{\Lambda}^d$  to compute the synthetic data used to construct  $\hat{\rho}_{\mathcal{D}}$  and  $N = 10^6$  samples from uniform prior on  $\Lambda$  to construct  $\tilde{\rho}_{p,\mathcal{D}}$ .

We apply the accept-reject algorithm to  $N = 40,000$  samples from uniform prior on  $\Lambda$ . The algorithm rejected 29,317 of these samples, which is typical for this example in repeated trials. In Fig. 14, we show the estimates  $\hat{\rho}_{\mathcal{D}}$  and  $\tilde{\rho}_{p,\mathcal{D}}$  and samples that are accepted by the algorithm.

We emphasize that the importance sampling and accept-reject methodologies are two different approaches for estimating the same solution.

## 6. Conclusion

In this paper, we consider the problem of solving an inverse problem in which a complex system is described by a computer model and system behavior is governed by parameters in the model but it is impossible to observe the values of the input parameters. So, they must be inferred using model evaluations and observations from the system. We formulate and solve the empirical Stochastic Inverse Problem, which is to determine a probability distribution for the parameters governing the system.

We develop and analyze a nonparametric Bayesian approach to defining a unique posterior distribution for the parameters given a prior. We prove that the solution exists and give a

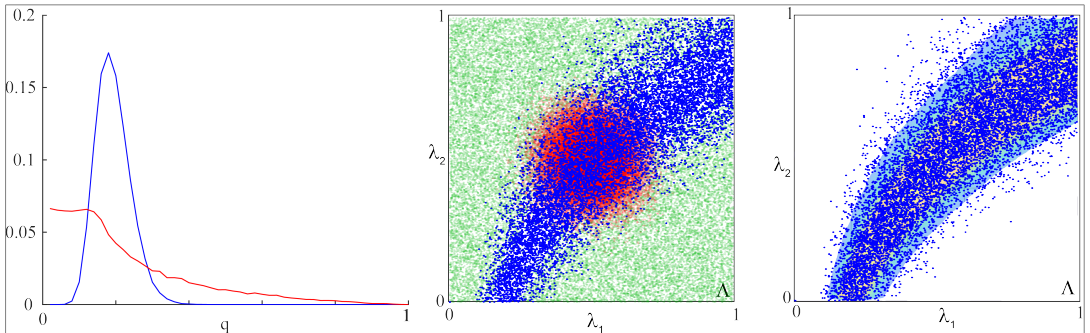


Fig 14. Left: Plots of  $\hat{p}_D$  (blue) and  $\hat{p}_{p,D}$  (red). Center: Scatter plots of samples from the data generating distribution (red), uniform prior (green), and the posterior distribution (blue). We see that the accepted samples lie in the “shadow” of the data generating distribution along the contours. Right: Scatter plot of uniform prior samples accepted by the accept-reject algorithm that are distributed according to the posterior distribution on top of the heatmap of the empirical posterior computed from re-weighting samples distributed according to the prior.

concrete expression for the solution using disintegration of measures. Conditions where the solution can be written in terms of conditional densities is developed, and we prove that under general conditions, the solution is continuous a.e. We also show that the solution corresponding to the uniform prior has maximum entropy. A nonparametric solution method based on random sampling is proposed, with an analysis of its accuracy and convergence properties, along with an alternative accept–reject method. Finally, we illustrate with a number of examples, including one that deals with the situation in which there is insufficient data for a nonparametric approach and a simulation-based inference approach is used.

Future work includes incorporating random effects to broaden the range of applications for the SIP framework, including linking the eSIP to classic Bayesian statistics and formulating and solving the eSIP for multiple experiments on one system. Another direction is the development of more comprehensive methods for situations where the available data is limited and simulation-based is required. Ongoing efforts also focus on extending SIP solutions to infinite-dimensional spaces and investigating the use of Markov Chain Monte Carlo methods and machine learning for the solution of the eSIP.

## Funding

L. Yang acknowledges the support of the United States Department of Energy and the United States National Science Foundation.

H. Shi acknowledges the support of the Natural Sciences and Engineering Research Council of Canada.

J. Chi acknowledges the support of the United States National Science Foundation.

T. Butler’s work is supported by the National Science Foundation under Grant No. DMS-2208460. However, any opinion, finding, and conclusions or recommendations expressed in this material are those of the author and do not necessarily reflect the views of the National Science Foundation.

H. Wang’s work is supported by the National Science Foundation

D. Bingham acknowledges the support of the Natural Sciences and Engineering Research Council of Canada.

D. Estep's work has been partially supported by the Canada Research Chairs Program, the Natural Sciences and Engineering Research Council of Canada, Canada's Digital Technology Superclustre, the Dynamics Research Corporation, the Idaho National Laboratory, the United States Department of Energy, the United States National Institutes of Health, the United States National Science Foundation, and Riverside Research.

## References

- [1] J. Anderson and S. Anderson. A Monte Carlo implementation of the nonlinear filtering problem to produce ensemble assimilations and forecasts. *Mon. Weather Rev.*, 127:2741 – 2758, 1999.
- [2] J. Annan, J. Hargreaves, N. Edwards, and R. Marsh. Parameter estimation in an intermediate complexity earth system model using an ensemble Kalman filter. *Ocean Model.*, 8(1):135–154, 2005.
- [3] R. N. Bannister. A review of operational methods of variational and ensemble-variational data assimilation. *Quart. J. Roy. Meteor. Soc.*, 143(703):607–633, 2017.
- [4] S. Basu, T. Butler, D. Estep, and P. Nishant. *A Ramble Through Probability: How I Learned to Stop Worrying and Love Measure Theory*. SIAM, Philadelphia, 2024.
- [5] S. Basu, F. Yazdi, A. Prasad, D. Estep, and D. Bingham. The constrained stochastic inverse problem for a random vector, 2025. in preparation.
- [6] D. Bingham, T. Butler, and D. Estep. Inverse problems for physics-based process models. *Ann. Rev. Stat. Appl.*, 11, 2024.
- [7] M. Biron-Lattes, P. Belliveau, F. Yazdi, S. Basu, D. Estep, D. Bingham, and D. Schouten. GPU-accelerated gradient-based MCMC inference for surface-based models of block cave mining, 2025. in preparation.
- [8] V.I. Bogachev. *Measure Theory*, volume 1-2. Springer-Verlag, New York, 2007.
- [9] J. Breidt, T. Butler, and D. Estep. A measure-theoretic computational method for inverse sensitivity problems I: Method and analysis. *SINUM*, 49:1836–1859, 2011.
- [10] T. Butler and D. Estep. A numerical method for solving a stochastic inverse problem for parameters. *Ann. Nucl. Energy*, 52:86–94, 2013.
- [11] T. Butler, D. Estep, and J. Sandelin. A computational measure theoretic approach to inverse sensitivity problems II: A posteriori error analysis. *SINUM*, 50:22–45, 2012.
- [12] T. Butler, D. Estep, S. Tavener, C. Dawson, and J.J. Westerink. A measure-theoretic computational method for inverse sensitivity problems III: Multiple quantities of interest. *SIAM/ASA JUQ*, 2:174–202, 2014.
- [13] T. Butler, L. Graham, D. Estep, C. Dawson, and J.J. Westerink. Definition and solution of a stochastic inverse problem for the Manning's  $n$  parameter field in hydrodynamic models. *Adv. in Water Resour.*, 78:60 – 79, 2015.
- [14] T. Butler, A. Huhtala, and M. Juntunen. Quantifying uncertainty in material damage from vibrational data. *JCP*, 283:414 – 435, 2015.
- [15] T. Butler, L. Graham, S. Mattis, and S. Walsh. A measure-theoretic interpretation of sample based numerical integration with applications to inverse and prediction problems under uncertainty. *SISC*, 39:A2072–A2098, 2017.
- [16] T. Butler, J. Jakeman, and T. Wildey. Combining push-forward measures and Bayes' rule to construct consistent solutions to stochastic inverse problems. *SISC*, 40:A984–A1011, 2018.

[17] T. Butler, J. Jakeman, and T. Wildey. Convergence of probability densities using approximate models for forward and inverse problems in uncertainty quantification. *SISC*, 40:A3523–A3548, 2018.

[18] T. Butler, T. Wildey, and T. Yen. Data-consistent inversion for stochastic input-to-output maps. *Inv. Prob.*, 36:085015, aug 2020.

[19] D. Calvetti, J. Kaipio, and E. Somersalo. Inverse problems in the Bayesian framework. *Inv. Prob.*, 30:110301, 2014.

[20] A. Carrassai, M. Bocquet, L. Bertino, and G. Evensen. Data assimilation in the geosciences: An overview of methods, issues, and perspectives. *WIREs Climate Change*, 9 (5):e535, 2018.

[21] J. Chang and D. Pollard. Conditioning as disintegration. *Stat. Neer.*, 51:287–317, 1997.

[22] J. Chi. Sliced inverse approach and domain recovery for stochastic inverse problems, 2021. Ph.D. Thesis, Department of Statistics, Colorado State University.

[23] A. Cioaca, A. Sandu, and E. de Sturler. Efficient methods for computing observation impact in 4D-Var data assimilation. *Comput. Geos.*, 17:975–990, 2013.

[24] S. Cotter, M. Dashti, and A. Stuart. Approximation of Bayesian inverse problems. *SINUM*, 48:322–345, 2010.

[25] L. Devroye and L. Györfi. *Nonparametric density estimation: the L1 view*. Wiley, New York, 1985.

[26] A. Doucet, S. Godsill, and C. Andrieu. On sequential Monte Carlo sampling methods for Bayesian filtering. *Stat. Comput.*, page 197–208, 2000.

[27] E. Epstein. Stochastic dynamic prediction. *Tellus*, 21:739–759, 1969.

[28] O. Ernst, B. Sprungk, and H. Starkloff. *Bayesian Inverse Problems and Kalman Filters*, pages 133–159. Springer International Publishing, Cham, 2014.

[29] L. Evans and R. Gariepy. *Measure Theory and Fine Properties of Functions*. CRC Press, New York, 2015.

[30] P. Fearnhead and H. Kunsch. Particle filters and data assimilation. *Annu. Rev. Statist. Appl.*, page 421–449, 2018.

[31] B. Fitzpatrick. Bayesian analysis in inverse problems. *Inv. Prob.*, 7:675, 1991.

[32] G. Folland. *Real analysis: Modern techniques and their applications*. John Wiley & Sons, 2013.

[33] E. Geir. The ensemble Kalman filter: Theoretical formulation and practical implementation. *Ocean Dyn.*, 53:343–367, 2003.

[34] S. Ghosal and A. van der Vaart. *Fundamentals of Nonparametric Bayesian Inference*. Cambridge University Press, New York, 2017.

[35] T. Gneiting, F. Balabdaoui, and A. Raftery. Probabilistic forecasts, calibration and sharpness. *JRSSS B*, 69:243–268, 2007.

[36] L. Graham, T. Butler, S. Walsh, C. Dawson, and J. Westerink. A measure-theoretic algorithm for estimating bottom friction in a coastal inlet: Case study of Bay St. Louis during Hurricane Gustav (2008). *Mon. Weath. Rev.*, 145:929–954, 2017.

[37] L. Graham, S. Mattis, S. Walsh, T. Butler, M. Pilosov, and D. McDougall. BET: Butler, Estep, Tavener Method v3.0.0, 2020. URL <https://doi.org/10.5281/zenodo.3936258>. Documentation: <http://ut-chg.github.io/BET/>.

[38] M. Grosskopf, D. Bingham, M. Adams, W.D. Hawkins, and D. Perez-Nunez. Generalized computer model calibration for radiation transport simulation. *Techno.*, 00, 2020.

- [39] D. Higdon, M. Kennedy, J. Cavendish, J. Cafeo, and R. Ryne. Combining field data and computer simulations for calibration and prediction. *SISC*, 26:448–466, 2004.
- [40] D. Higdon, J. Gattiker, B. Williams, and M. Rightley. Computer model calibration using high-dimensional output. *JASA*, 103:570–583, 2008.
- [41] M. Hirsch. *Differential Topology*. Springer, 1976.
- [42] J. Hoffman-Jorgensen. *Probability with a View Towards Statistics*, volume 1-2. Academic Press, Inc., New York, 1994.
- [43] N. Janani, K. Young, G. Kinney, M. Strand, J. Hokanson, Y. Liu, T. Butler, and E. Austin. A novel application of data-consistent inversion to overcome spurious inference in genome-wide association studies. *Genetic Epi.*, pages 270–288, 2024.
- [44] O. Kallenberg. *Foundations of Modern Probability*. Springer, New York, 2002.
- [45] M. Kennedy and A. O’Hagan. Bayesian calibration of computer models. *JSSB*, 63:425–464, 2001.
- [46] E. Khmaladze and N. Toronjadze. On the almost sure coverage property of Voronoi tessellation: The  $\mathbb{R}^1$  case. *Adv. Appl. Prob.*, 33:756–764, 2001.
- [47] K. Kroetch and D. Estep. Bayesian inverse ensemble forecasting for COVID-19. *Can. J. Stat.*, pages 1–40, 2025. in revision.
- [48] J. Lee. *Introduction to smooth manifolds*, volume 218. Springer Science & Business Media, 2012.
- [49] P. Lermusiaux. Uncertainty estimation and prediction for interdisciplinary ocean dynamics. *J. Comput. Phys.*, 217:176–199, 2006.
- [50] M. Leutbecher and T. N. Palmer. Ensemble forecasting. *JCP*, 227:3515–3539, 2008.
- [51] J. Lewis. Roots of ensemble forecasting. *Mon. Wea. Rev.*, 133:1865–1885, 2005.
- [52] L. Lin, D. Bingham, F. Broekgaarden, and I. Mandel. Uncertainty quantification of a computer model for binary black hole formation. *Annals Appl. Stat.*, 15(4):1604–1627, 2021.
- [53] S. Mattis, T. Butler, C. Dawson, D. Estep, and V. Vesselinov. Parameter estimation and prediction for groundwater contamination based on measure theory. *Water Resour. Res.*, 51:7608–7629, 2015.
- [54] S. Mattis, K. Steffen, T. Butler, C. Dawson, and D. Estep. Learning quantities of interest from dynamical systems for observation-consistent inversion. *CMAME*, 388:114230, 2022. ISSN 0045-7825.
- [55] C. Nave. HyperPhysics, 2024. URL <http://www.hyperphysics.phy-astr.gsu.edu/hbase/hframe.html>. Hosted by the Department of Physics and Astronomy, Georgia State University.
- [56] R. Palmer. The ECMWF ensemble prediction system: Looking back (more than) 25 years and projecting forward 25 years. *Quart. J. Roy. Met. Soc.*, 145:12–24, 2019.
- [57] M. Penrose. Laws of large numbers in stochastic geometry with statistical applications. *Bernoulli*, 13:1124–1150, 2007.
- [58] M. Plumlee. Bayesian calibration of inexact computer models. *JASA*, 112:1274–1285, 2017.
- [59] M. Rao. *Conditional Measures and Applications*. Chapman & Hall, New York, 2005.
- [60] W. Rudin. *Principles of mathematical analysis*. McGraw-hill New York, 1964.
- [61] W. Rudin. *Real and complex analysis*. Tata McGraw-Hill Education, 1987.
- [62] D. Sanz-Alonso, A. Stuart, and A. Taeb. *Inverse Problems and Data Assimilation*. Cambridge University Press, Cambridge, UK, 2023.

[63] A. Sard. Hausdorff measure of critical images on Banach manifolds. *Am. J. Math.*, 87: 158–174, 1965.

[64] M. Schervish. *Theory of Statistics*. Springer, New York, 1995.

[65] H. Schlichtkrull. Differentiable manifolds, lecture notes for geometry 2. *University of Copenhagen, Department of Mathematics, link: www.math.ku.dk/ jakobsen/geom2/manusgeom2.pdf*, 2013.

[66] H. Shi and D. Estep. The condition numbers of stochastic inverse problems, 2025. in preparation.

[67] P. B. Stark and L. Tenorio. *A Primer of Frequentist and Bayesian Inference in Inverse Problems*, pages 9–32. John Wiley & Sons, Ltd, 2010. ISBN 9780470685853.

[68] D. Stoyan, W. Kendall, and J. Mecke. *Stochastic Geometry and Its Applications*. John Wiley & Sons, New York, 1999.

[69] A. Stuart. Inverse problems: A Bayesian perspective. *Acta Num.*, 19:451–559, 2010.

[70] A. Tarantola. *Inverse Problem Theory and Methods for Model Parameter Estimation*. SIAM, Philadelphia, 2005.

[71] R. Tuo and J. Wu. Efficient calibration for imperfect computer models. *Ann. Statist.*, 43:2331–2352, 12 2015.

[72] P. van Leeuwen, H. Künsch, L. Nerger, R. Potthast, and S. Reich. Particle filters for high-dimensional geoscience applications: A review. *Quar. J. Roy. Meteor. Soc.*, 145 (723):2335–2365, 2019.

[73] J. Wilson. The definition of a manifold and first examples. *Stanford University, Department of Mathematics, link: https://web.stanford.edu/ jchw/WOMPtalk-Manifolds.pdf*, 2012.

[74] L. Yang. Infinite dimensional stochastic inverse problems, 2018. Ph.D. Thesis, Department of Statistics, Colorado State University.

[75] F. Yazdi, S. Basu, D. Estep, D. Bingham, and D. Schouten. Bayesian inversion and uncertainty quantification for muon tomography. *J. Appl. Geophysics*, 2024. submitted.

[76] E. Zauderer. *Partial Differential Equations of Applied Mathematics*. Wiley, New York, 2006.

[77] J. Zhu and D. Estep. An efficient and accurate machine learning method for computing probability of failure. *ASA DSiS*, pages 1–35, 2014. in revision.

[78] J. Zhu and D. Estep. Solution of the stochastic inverse problem by machine learning algorithms for multiple classifications, 2025. in preparation.

## Appendix A: Proofs

### A.1. Proof of Theorem 2.6

The result follows from the Implicit Function Theorem [60].

**Theorem A.1.** *Let  $f$  be a continuously differentiable map of  $U \times V \subset \mathbb{R}^{n_1+n_2} \rightarrow \mathbb{R}^{n_1}$ , where  $U \subset \mathbb{R}^{n_1}$  and  $V \subset \mathbb{R}^{n_2}$  are open sets. Assume  $f(\bar{x}, \bar{y}) = 0$  for a point  $(\bar{x}, \bar{y}) \in U \times V$ . Set  $A_x = J_{f,x}(\bar{x}, \bar{y})$  and  $A_y = J_{f,y}(\bar{x}, \bar{y})$  and assume  $A_x$  is invertible.*

*There exist open sets  $\mathring{U} \subset U$  and  $\mathring{V} \subset V$ , with  $(\bar{x}, \bar{y}) \in \mathring{U} \times \mathring{V}$ , such that for every  $y \in \mathring{V}$  there is a unique  $x \in \mathring{U}$  with  $f(x, y) = 0$ . This defines a continuously differentiable map  $x = g(y)$  of  $\mathring{V}$  into  $\mathring{U}$  such that  $f(g(y), y) = 0$  for  $y \in \mathring{V}$  satisfying  $\bar{x} = g(\bar{y})$  and  $J_g(\bar{y}) = -(A_x)^{-1}A_y$ .*

A **regular parameterized manifold in  $\mathbb{R}^n$**  is a map  $g : U \rightarrow \mathbb{R}^n$ , where  $U \subset \mathbb{R}^k$  is a non-empty open set, such that the  $n \times k$  Jacobian matrix  $J_g(x)$  has rank  $k$  at all  $x \in U$  [41, 48, 63, 65, 73]. If a map  $g : A \rightarrow B$ , where  $A \subset \mathbb{R}^k$  and  $B \subset \mathbb{R}^n$ , is continuous, bijective and has a continuous inverse it is called a **homeomorphism**. A regular parameterized manifold  $g : U \rightarrow \mathbb{R}^n$ , where  $U \subset \mathbb{R}^k$  is a non-empty open set, that is a homeomorphism is called an **embedded parameterized manifold**.

A  $k$ -dimensional manifold in  $\mathbb{R}^n$  is locally a  $k$ -dimensional embedded parameterized manifold. Specifically, a  **$k$ -dimensional manifold** is a non-empty set  $C \subset \mathbb{R}^n$  such that each point  $p \in C$  there is an open neighborhood  $N(p)$  of  $p$  and an  $k$ -dimensional embedded parameterized manifold  $g : U \rightarrow \mathbb{R}^n$  such that  $g(U) = C \cap N(p)$ . Equivalently, a non-empty set  $C \subset \mathbb{R}^n$  is an  $k$ -dimensional manifold if and only there is an open neighborhood  $N(p)$  of  $p$ , such that  $C \cap N(p)$  is the graph of a function  $g$ , where  $n - k$  of the variables  $x_1, \dots, x_n$  are functions of the other  $k$  variables.

The application of these concepts is straightforward given Assumptions 2.1 and 2.5, and Theorem A.1 implies Theorem 2.6.

We recall that every continuously differentiable manifold is diffeomorphic to a continuously infinitely differentiable manifold, so we simply say that generalized contours are locally smooth  $n - d$ -dimensional manifolds. It further follows that  $Q^{-1}(q)$  is locally approximated by the Jacobian of  $Q^{-1}$  at each point, where the Jacobian is surjective a.e. A manifold with these properties is called a **submersion**.

## A.2. Proof of Theorem 2.9.

Under Assumptions 2.1 and 2.5, we may write the solution of the SIP in terms of conditional densities with respect to the underlying Lebesgue measures. The proof of Theorem 2.9 depends on describing how  $Q$  transforms the Lebesgue measure. We denote the Lebesgue measure on  $(\Lambda, \mathcal{B}_\Lambda)$  by  $\mu_\Lambda$  and the Lebesgue measure on  $(\mathcal{D}, \mathcal{B}_\mathcal{D})$  by  $\mu_\mathcal{D}$ . We define the  $Q$ -induced measure  $\tilde{\mu}_\mathcal{D}$  on  $(\mathcal{D}, \mathcal{B}_\mathcal{D})$  by  $\tilde{\mu}_\mathcal{D}(A) = Q\mu_\Lambda = \mu_\Lambda(Q^{-1}(A))$  for  $A \in \mathcal{B}_\mathcal{D}$ .

The following result gives conditions that imply that  $\tilde{\mu}_\mathcal{D}$  is absolutely continuous with respect to  $\mu_\mathcal{D}$  with density that involves a surface integral over each contour  $Q^{-1}(y)$ .

**Theorem A.2.** *Assume Assumptions 2.1 and 2.5 hold. Let  $\nu_\Lambda$  be a measure on  $(\Lambda, \mathcal{B}_\Lambda)$  that is absolutely continuous with respect to  $\mu_\Lambda$  so  $d\nu_\Lambda = f_\Lambda d\mu_\Lambda$  for a nonnegative measurable function  $f_\Lambda$ . Let  $\tilde{\nu}_\mathcal{D} = Q\nu_\Lambda$ . Then,  $d\tilde{\nu}_\mathcal{D} = \tilde{f}_\mathcal{D}(q) d\mu_\mathcal{D}$ , where*

$$\tilde{f}_\mathcal{D}(q) = \int_{Q^{-1}(q)} f_\Lambda \frac{1}{\sqrt{\det(J_Q J_Q^\top)}} ds. \quad (\text{A.1})$$

In the case that  $\nu_\Lambda = \mu_\Lambda$ , then  $d\tilde{\mu}_\mathcal{D} = \tilde{\rho}_\mathcal{D}(q) d\mu_\mathcal{D}$ , where

$$\tilde{\rho}_\mathcal{D}(q) = \int_{Q^{-1}(q)} \frac{1}{\sqrt{\det(J_Q J_Q^\top)}} ds. \quad (\text{A.2})$$

Moreover,  $\tilde{\rho}_\mathcal{D}(q) > 0$  for almost all  $q \in \mathcal{D}$  with  $Q^{-1}(q) \subset \text{int } \Lambda$ , where  $\text{int } \Lambda$  is the interior of  $\Lambda$ . If  $\mu_\mathcal{D}(Q(\Lambda) \setminus Q(\text{int } \Lambda)) = 0$ , then  $\mu_\mathcal{D}(\{q \in \mathcal{D}, \tilde{\rho}_\mathcal{D}(q) = 0\}) = 0$ .

*Proof.* We start by showing (A.2). We prove that for any generalized rectangle  $[a, b] \subset \mathbb{R}^m$  with  $b > a$ ,

$$\tilde{\mu}_{\mathcal{D}}([a, b]) = \int_{[a, b]} \int_{Q^{-1}(q)} \frac{1}{\sqrt{\det(J_Q J_Q^\top)}} ds d\mu_{\mathcal{D}}(q).$$

The result follows from the Caratheodory Extension Theorem [4].

Without loss of generality, we assume that  $J_Q$  is full rank for every  $\lambda \in Q^{-1}([a, b])$ . This implies there are  $m$  indices  $i_1, i_2, \dots, i_m \in \{1, 2, \dots, m\}$  such that  $J_Q^{(m)} = (J_Q^{i_1} \ J_Q^{i_2} \ \dots \ J_Q^{i_m})$  is invertible at  $\lambda$ , where  $J_Q^i = i^{th}$  column of  $J_Q$ . Since  $J_Q$  is continuous, there is an open ball  $B_r(\lambda)$  of radius  $r$  centered at  $\lambda$ , such that  $J_Q^{(m)}$  is invertible in  $B_r(\lambda) \cap Q^{-1}([a, b])$ .

$Q^{-1}([a, b])$  is a compact subset of  $\Lambda$ . We choose a finite collection  $U_j = B_{r_j}(\lambda_j)$ ,  $j = 1, \dots, J$ , such that  $Q^{-1}([a, b]) \subset \bigcup_{j=1}^J U_j$ . We make the replacements  $U_1 \leftarrow U_1$  and, for  $j > 1$ ,  $U_j \leftarrow U_j \setminus \overline{(\bigcup_{k=1}^{j-1} U_k)}$ . We obtain a disjoint collection of open sets  $\{U_j\}_{j=1}^J$  that covers  $Q^{-1}([a, b])$  except possibly for a negligible set.

In  $U_j \cap Q^{-1}([a, b])$ ,  $1 \leq j \leq J$ , we may write  $(\lambda) \sim (\lambda^{(m_j)}; \hat{\lambda}^{(m_j)})$  of which  $\lambda^{(m_j)}$  are  $m$  coordinates of  $\lambda$  for which the Jacobian  $J_Q^{(m_j)}$  is invertible, and  $\hat{\lambda}^{(m_j)}$  the remaining  $n - m$  entries with Jacobian  $\hat{J}_Q^{(m_j)}$ . We define  $\pi_j : \mathbb{R}^n \rightarrow \mathbb{R}^{n-m}$  to be  $\pi_j(\lambda) = \hat{\lambda}^{(m_j)}$ ,  $V_j = \{(Q(\lambda), \pi_j(\lambda)); \lambda \in U_j \cap Q^{-1}([a, b])\}$ , and  $V_{jq} = \{\pi_j(\lambda); \lambda \in Q^{-1}(q) \cap U_j\}$  for any  $q \in [a, b]$ .

Temporarily, we fix  $j$  and drop the subscript on  $M$ .  $V_j$  is diffeomorphic to  $U_j \cap Q^{-1}([a, b])$  and

$$d\lambda^{(m)} \ d\hat{\lambda}^{(m)} = \left| \det(J_Q^{(m)})^{-1} \right| d\mu_{\mathcal{D}}(q) d\hat{\lambda}^{(m)}.$$

For fixed  $q$ , Theorem A.1 implies that for each  $U_j$ , there is a continuously differentiable map  $f$  such that  $\lambda^{(m)} = f(\hat{\lambda}^{(m)})$ . The map  $f$  has Jacobian  $J_f = (J_Q^{(m)})^{-1} \hat{J}_Q^{(m)}$  so, under any suitable parameterization, the differential form on the manifold  $Q^{-1}(q) \cap U_j$  can be written

$$ds = \sqrt{\det((J_Q^{(m)})^{-1} \hat{J}_Q^{(m)}, I) ((J_Q^{(m)})^{-1} \hat{J}_Q^{(m)}, I)^\top} d\hat{\lambda}^{(m)} = k(\lambda) d\hat{\lambda}^{(m)},$$

where  $k(\lambda) = \sqrt{\det(J_Q J_Q^\top)} \left| \det(J_Q^{(m)})^{-1} \right|$ . Therefore

$$\begin{aligned} \tilde{\mu}_{\mathcal{D}}([a, b]) &= \mu_{\Lambda}(Q^{-1}([a, b])) = \sum_{j=1}^J \mu_{\Lambda}(U_j \cap Q^{-1}([a, b])) \\ &= \sum_{j=1}^J \int_{U_j \cap Q^{-1}([a, b])} d\lambda_i^{(m_j)} d\hat{\lambda}_i^{(m_j)} = \sum_{j=1}^J \int_{V_j} \left| \det(J_Q^{(m_j)})^{-1} \right| d\hat{\lambda}_i^{(m_j)} d\mu_{\mathcal{D}}(q) \\ &= \int_{[a, b]} \sum_{j=1}^J \int_{V_{jq}} \left| \det(J_Q^{(m_j)})^{-1} \right| d\hat{\lambda}_i^{(m)} d\mu_{\mathcal{D}}(q) \\ &= \int_{[a, b]} \sum_{j=1}^J \int_{V_{jq}} \frac{1}{\sqrt{\det(J_Q J_Q^\top)}} ds d\mu_{\mathcal{D}}(q) = \int_{[a, b]} \int_{Q^{-1}(q)} \frac{1}{\sqrt{\det(J_Q J_Q^\top)}} ds d\mu_{\mathcal{D}}(q). \end{aligned}$$

If  $q \in \mathcal{D}$ , and  $Q^{-1}(q) \subset \text{int } \Lambda$ , there exists  $\lambda \in \text{int } \Lambda$  such that  $Q(\lambda) = q$ . So there exists a neighborhood  $N(\lambda)$  of  $\lambda$  with  $N(\lambda) \subset \text{int } \Lambda$ . Since  $Q^{-1}(q) \cap N(\lambda)$  is diffeomorphic to an open set in  $\mathbb{R}^{n-m}$ ,

$$\tilde{\rho}_{\mathcal{D}}(q) > \int_{Q^{-1}(q) \cap N(\lambda)} \frac{1}{\sqrt{\det(J_Q J_Q^\top)}} ds > 0.$$

This argument also shows that if  $q \in Q(\Lambda)$  satisfies  $\tilde{\rho}_{\mathcal{D}}(q) = 0$  then  $q \in Q(\Lambda) \setminus Q(\text{int } \Lambda)$ .

Next, we address the general case. First we assume  $f_\Lambda$  is a simple function, i.e.,  $f_\Lambda(\lambda) = \sum_{i=1}^k a_i \chi_{A_i}(\lambda)$  for positive numbers  $\{a_i\}_{i=1}^k$  and partition  $\{A_i\}_{i=1}^k \subset \mathcal{B}_\Lambda$  of  $\Lambda$ . For any  $B \in \mathcal{B}_{\mathcal{D}}$ , we have

$$\begin{aligned} \nu_\Lambda(Q^{-1}(B)) &= \sum_{i=1}^k a_i \mu_\Lambda(Q^{-1}(B) \cap A_i) \\ &= \sum_{i=1}^k a_i \int_{B \cap Q(A_i)} \int_{Q^{-1}(q) \cap A_i} \frac{1}{\sqrt{\det(J_Q J_Q^\top)}} ds d\mu_{\mathcal{D}}(q) \\ &= \sum_{i=1}^k a_i \int_B \int_{Q^{-1}(q) \cap A_i} \frac{1}{\sqrt{\det(J_Q J_Q^\top)}} ds d\mu_{\mathcal{D}}(q) \\ &= \int_B \int_{Q^{-1}(q)} \sum_{i=1}^k a_i \chi_{A_i}(\lambda) \frac{1}{\sqrt{\det(J_Q J_Q^\top)}} ds d\mu_{\mathcal{D}}(q) \\ &= \int_B \int_{Q^{-1}(q)} f_\Lambda(\lambda) \frac{1}{\sqrt{\det(J_Q J_Q^\top)}} ds d\mu_{\mathcal{D}}(q). \end{aligned}$$

We approximate a general nonnegative measurable function  $f_\Lambda$  by a pointwise convergent monotone sequence of simple functions and use the Monotone Convergence Theorem to pass to a limit and obtain the result [4].

□

We now are in position to prove the main result.

*Proof of Theorem 2.9.*  $P_p$  defines an a.e. unique Ansatz prior  $\{P_{p,N}(\cdot|q)\}_{q \in \mathcal{D}}$  via the disintegration,

$$P_p(A) = \int_{Q(A)} P_{p,N}(A|q) d\tilde{P}_{p,\mathcal{D}}(q) = \int_{Q(A)} \int_{Q^{-1}(q) \cap A} dP_{p,N}(\lambda|q) d\tilde{P}_{p,\mathcal{D}}(q) \quad (\text{A.3})$$

for all  $A \in \mathcal{B}_\Lambda$ , where  $P_{p,N}(\cdot|q)$  is concentrated on  $Q^{-1}(q)$ . We note that Assumption 2.8 implies that  $\tilde{\rho}_{p,\mathcal{D}}(q) > 0$  for all  $q \in \mathcal{D}$ . Using (2.5), (2.8), and Theorem A.2, we have

$$\begin{aligned} P_\Lambda(A) &= \int_{Q(A)} \int_{Q^{-1}(q) \cap A} dP_{p,N}(\lambda|q) dP_{\mathcal{D}}(q) \\ &= \int_{Q(A)} \int_{Q^{-1}(q) \cap A} dP_{p,N}(\lambda|q) \frac{\rho_{\mathcal{D}}(q)}{\tilde{\rho}_{p,\mathcal{D}}(q)} d\tilde{P}_{p,\mathcal{D}}(q) \\ &= \int_A \frac{\rho_{\mathcal{D}}(Q(\lambda))}{\tilde{\rho}_{p,\mathcal{D}}(Q(\lambda))} dP_p = \int_A \frac{\rho_{\mathcal{D}}(Q(\lambda))}{\tilde{\rho}_{p,\mathcal{D}}(Q(\lambda))} \rho_p d\mu_\Lambda. \end{aligned}$$

The density  $\frac{\rho_{\mathcal{D}}(Q(\lambda))\rho_p(\lambda)}{\tilde{\rho}_{p,\mathcal{D}}(Q(\lambda))}$  is unique  $\mu_{\Lambda}$  a.e. □

### A.3. Proof of Theorem 2.10

*Proof.* Let  $P_{\Lambda}$  be the solution of the SIP corresponding any prior  $P_p$  and let  $\bar{P}_{\Lambda}$  denote the solution corresponding to the uniform prior. By Theorem 2.9, these have respective densities,

$$\rho_{\Lambda}(\lambda) = \frac{\rho_{\mathcal{D}}(Q(\lambda))}{\tilde{\rho}_{p,\mathcal{D}}(Q(\lambda))} \cdot \rho_p(\lambda), \quad \bar{\rho}_{\Lambda}(\lambda) = \frac{\rho_{\mathcal{D}}(Q(\lambda))}{\tilde{\rho}_{\mathcal{D}}(Q(\lambda))},$$

since  $\bar{\rho}_{\Lambda}(\lambda) = 0$  implies  $\rho_{\Lambda}(\lambda) = 0$ . We compute

$$\begin{aligned} D(\rho_{\Lambda} \parallel \bar{\rho}_{\Lambda}) &= \int_{\Lambda} \rho_{\Lambda}(\lambda) \log \left( \frac{\rho_{\Lambda}(\lambda)}{\bar{\rho}_{\Lambda}(\lambda)} \right) d\mu_{\Lambda}(\lambda) \\ &= \int_{\Lambda} \rho_{\Lambda}(\lambda) \log(\rho_{\Lambda}(\lambda)) d\mu_{\Lambda}(\lambda) - \int_{\Lambda} \rho_{\Lambda}(\lambda) \log \left( \frac{1}{\bar{\rho}_{\Lambda}(\lambda)} \right) d\mu_{\Lambda}(\lambda) \\ &= -H(\rho_{\Lambda}) + H(\rho_{\Lambda}, \bar{\rho}_{\Lambda}). \end{aligned}$$

By (A.1),

$$\begin{aligned} H(\rho_{\Lambda}, \bar{\rho}_{\Lambda}) &= \int_{\mathcal{D}} \int_{Q^{-1}(q)} \rho_{\Lambda}(\lambda) \log \left( \frac{1}{\bar{\rho}_{\Lambda}(\lambda)} \right) \frac{1}{\sqrt{\det(J_Q J_Q^{\top})}} ds d\mu_{\mathcal{D}}(q) \\ &= \int_{\mathcal{D}} \int_{Q^{-1}(q)} \frac{\rho_{\mathcal{D}}(Q(\lambda))}{\tilde{\rho}_{p,\mathcal{D}}(Q(\lambda))} \rho_p(\lambda) \cdot \log \left( \frac{\tilde{\rho}_{\mathcal{D}}(Q(\lambda))}{\rho_{\mathcal{D}}(Q(\lambda))} \right) \frac{1}{\sqrt{\det(J_Q J_Q^{\top})}} ds d\mu_{\mathcal{D}}(q). \end{aligned}$$

Rearranging and using (A.1),

$$\begin{aligned} H(\rho_{\Lambda}, \bar{\rho}_{\Lambda}) &= \int_{\mathcal{D}} \frac{\rho_{\mathcal{D}}(q)}{\tilde{\rho}_{p,\mathcal{D}}(q)} \log \left( \frac{\tilde{\rho}_{\mathcal{D}}(q)}{\rho_{\mathcal{D}}(q)} \right) \left( \int_{Q^{-1}(q)} \rho_p(\lambda) \frac{1}{\sqrt{\det(J_Q J_Q^{\top})}} ds \right) d\mu_{\mathcal{D}}(q) \\ &= \int_{\mathcal{D}} \rho_{\mathcal{D}}(q) \log \left( \frac{\tilde{\rho}_{\mathcal{D}}(q)}{\rho_{\mathcal{D}}(q)} \right) d\mu_{\mathcal{D}}(q) = \int_{\Lambda} \bar{\rho}_{\Lambda}(\lambda) \log \left( \frac{1}{\bar{\rho}_{\Lambda}(\lambda)} \right) d\mu_{\Lambda}(\lambda) = H(\bar{\rho}_{\Lambda}). \end{aligned}$$

We conclude that  $H(\bar{\rho}_{\Lambda}) - H(\rho_{\Lambda}) = D(\rho_{\Lambda} \parallel \bar{\rho}_{\Lambda}) \geq 0$ . □

### A.4. Proof of Theorem 2.12

For simplicity of notation, we prove the result for the uniform prior. The general result follows using the same proof with minor alterations. We first prove a special case.

**Theorem A.3.** *Assume Assumptions 2.1, 2.5, and 2.11 hold. For  $q_0 \in \mathcal{D}$ , assume that*

1. *There exists  $\{i_1, \dots, i_m\} \subset \{1, \dots, n\}$  such that  $J_Q^{(m)} = (J_Q^{(i_1)}, J_Q^{(i_2)}, \dots, J_Q^{(i_m)})$  is full rank on  $Q^{-1}(q_0)$ ,*
2.  *$(J_Q J_B)^{\top}$  is full rank on  $\partial\Lambda \cap Q^{-1}(q_0)$ .*

Then,  $\tilde{\rho}_{\mathcal{D}}(q)$  is continuous in a neighborhood of  $q_0$ .

*Proof.* Without loss of generality, we assume  $i_1 = 1, i_2 = 2, \dots, i_m = m$ . We let  $\lambda^{(m)} = (\lambda_1, \dots, \lambda_m)$ ,  $\hat{\lambda}^{(m)} = (\lambda_{m+1}, \dots, \lambda_n)$ , so  $\lambda$  can be formally written as  $\lambda \sim (\lambda^{(m)}, \hat{\lambda}^{(m)})$ . We define  $\pi_{\hat{m}} : \mathbb{R}^n \rightarrow \mathbb{R}^{n-m}$  as  $\pi_{\hat{m}}(\lambda) = \hat{\lambda}^{(m)}$ .

For a  $\lambda_0 \in \Lambda \cap Q^{-1}(q_0)$ , since  $J_Q^{(m)}(\lambda_0)$  is full rank, Theorem A.1 implies that  $Q(\lambda) - q = 0$  determines a unique continuous function  $h : N(\hat{\lambda}_0^{(m)}, r) \times N(q_0, r) \rightarrow N(\lambda_0^{(m)}, r)$ . Without loss of generality we assume  $h$  is defined on  $\overline{N(\hat{\lambda}_0^{(m)}, r)} \times \overline{N(q_0, r)}$ . Since the collection  $\{N(\hat{\lambda}^{(m)}, r) \times N(\lambda^{(m)}, r)\}$  covers the compact set  $\Lambda \cap Q^{-1}(q_0)$ , there is a finite subcover  $\{N(\hat{\lambda}_k^{(m)}, r_k) \times N(\lambda_k^{(m)}, r_k)\}, k = 1, \dots, K$ . Let  $r_0 = \min_k r_k$ . There is a unique continuous function  $h : \left( \bigcup_{k=1}^K \overline{N(\hat{\lambda}_k^{(m)}, r_k)} \right) \times \overline{N(q_0, r_0)} \rightarrow \bigcup_{k=1}^K N(\lambda_k^{(m)}, r_k)$ . We have

$$\tilde{\rho}_{\mathcal{D}}(q_0) = \int_{\pi_{\hat{m}}(\Lambda \cap Q^{-1}(q_0))} \frac{1}{\left| J_Q^{(m)}(h(\hat{\lambda}^{(m)}, q_0), \hat{\lambda}^{(m)}) \right|} d\hat{\lambda}^{(m)}.$$

Since  $J_Q^{(m)}(\lambda)$  is a continuous function,  $\left| J_Q^{(m)}(h(\hat{\lambda}^{(m)}, y), \hat{\lambda}^{(m)}) \right|^{-1}$  is continuous on a compact domain  $\left( \bigcup_{k=1}^K \overline{N(\hat{\lambda}_k^{(m)}, r_k)} \right) \times \overline{N(q_0, r_0)}$ , which means it is uniformly continuous and bounded. Let  $M > 0$  be bound so  $\left| J_Q^{(m)}(h(\hat{\lambda}^{(m)}, y), \hat{\lambda}^{(m)}) \right|^{-1} < M$ .

Since  $\partial\Lambda$  is piecewise smooth, for almost all  $\lambda_0 \in \partial\Lambda$ , there exists  $r$  such that  $B : N(\lambda_0, r) \rightarrow \mathbb{R}$  is a continuously differentiable map and determines  $\partial\Lambda \cap N(\lambda_0, r)$  by  $B(\lambda) = 0$ .

Take one such point  $\lambda_0 \in \partial\Lambda \cap Q^{-1}(q_0)$ , then there exists  $N(\lambda_0, r)$  such that  $\partial\Lambda \cap Q^{-1}(q_0)$  is determined by  $Q^*(\lambda) = \begin{pmatrix} Q(\lambda) - q_0 \\ B(\lambda) \end{pmatrix} = 0$  with

$$J_{Q^*} = \begin{pmatrix} J_Q \\ J_B \end{pmatrix} = \begin{pmatrix} J_Q^{(m)} & \hat{J}_Q^{(m)} \\ J_B^{(m)} & \hat{J}_B^{(m)} \end{pmatrix}$$

having full rank because of Condition 2. Since  $J_{Q^*}(\lambda_0)$  and  $J_Q^{(m)}(\lambda_0)$  are full rank, there exists  $j \in m+1, \dots, n$  such that

$$\begin{pmatrix} J_Q^{(m)} & (\hat{J}_Q^{(m)})_j \\ J_B^{(m)} & (\hat{J}_B^{(m)})_j \end{pmatrix}(\lambda_0)$$

is invertible.

Define  $\lambda^{(m+1)} = (\lambda^{(m)}, \lambda_j)$ ,  $\hat{\lambda}^{(m+1)} = \hat{\lambda}^{(m)} \setminus \lambda_j$ , where we write  $\lambda \sim (\lambda^{(m+1)}, \hat{\lambda}^{(m+1)})$ . By Theorem A.1, there exists a unique continuous function,

$$g : N(\hat{\lambda}_0^{(m+1)}, r') \times N(q_0, r') \rightarrow N(\lambda_0^{(m)}, r') \times N(\lambda_{0j}, r'),$$

which satisfies  $\overline{Q^*(g(\hat{\lambda}^{(m+1)}, y), \lambda^{(m)}, \lambda_j)} = 0$ . Without loss of generality, we assume  $g$  is defined on  $\overline{N(\hat{\lambda}_0^{(m+1)}, r')} \times \overline{N(q_0, r')}$ . By compactness of the domain,  $g$  is uniformly continuous. The set  $\{N(\hat{\lambda}^{(m+1)}, r') \times N(\lambda^{(m)}, r') \times N(\lambda_j, r')\}$  covers  $\partial\Lambda \cap Q^{-1}(y)$  for  $y \in N(q_0, r')$ .

We assume  $r'$  is sufficiently small so that

$$N(\hat{\lambda}^{(m+1)}, r') \times N(\lambda^{(m)}, r') \times N(\lambda_j, r') \subset \bigcup_{k=1}^K \left( N(\hat{\lambda}_k^{(m)}, r_k) \times N(\lambda_k^{(m)}, r_k) \right).$$

Since  $\partial\Lambda \cap Q^{-1}(q_0)$  is compact, there is a finite subcover  $\{N(\hat{\lambda}_\ell^{(m+1)}, r'_\ell) \times N(\lambda_\ell^{(m)}, r'_\ell) \times N(\lambda_{\ell j}, r'_\ell)\}$ ,  $\ell = 1, \dots, L$ . Let  $r'_0 = \min\{r'_\ell, \ell = 1, \dots, L; r_0\}$  then for any  $y \in N(q_0, r'_0)$ , the sets also cover  $\partial\Lambda \cap Q^{-1}(y)$ . So Condition 2 holds for all  $y \in N(q_0, r'_0)$ . Thus

$$\bigcup_{\ell=1}^L \left( N(\hat{\lambda}_\ell^{(m+1)}, r'_\ell) \times N(\lambda_\ell^{(m)}, r'_\ell) \times N(\lambda_{\ell j}, r'_\ell) \times N(q_0, r'_0) \right)$$

is covered by  $\{N(\hat{\lambda}_k^{(m)}, r_k) \times N(\lambda_k^{(m)}, r_k) \times N(q_0, r_0)\}$ .

As a result,  $\{N(\hat{\lambda}_k^{(m)}, r_k) \times N(\lambda_k^{(m)}, r_k)\}$  covers  $\Lambda \cap Q^{-1}(y)$  for all  $y \in N(q_0, r'_0)$ . Thus,

$$\tilde{\rho}_{\mathcal{D}}(y) = \int_{\pi_{\hat{m}}(\Lambda \cap Q^{-1}(y))} \frac{1}{\left| J_Q^{(m)}(h(\hat{\lambda}^{(m)}, y), \hat{\lambda}^{(m)}) \right|} d\hat{\lambda}^{(m)}.$$

For  $y \in N(q_0, r'_0)$ , let  $C = \pi_{\hat{m}}(\Lambda \cap Q^{-1}(q_0)) \Delta \pi_{\hat{m}}(\Lambda \cap Q^{-1}(y))$ . Thus,

$$|\tilde{\rho}_{\mathcal{D}}(q_0) - \tilde{\rho}_{\mathcal{D}}(q)|$$

$$\begin{aligned} &\leq \int_{\pi_{\hat{m}}(\Lambda \cap Q^{-1}(q_0))} \left| \frac{1}{\left| J_Q^{(m)}(h(\hat{\lambda}^{(m)}, q_0), \hat{\lambda}^{(m)}) \right|} - \frac{1}{\left| J_Q^{(m)}(h(\hat{\lambda}^{(m)}, q), \hat{\lambda}^{(m)}) \right|} \right| d\hat{\lambda}^{(m)} \\ &\quad + \int_C M d\hat{\lambda}^{(m)}. \end{aligned}$$

For the first term, uniform continuity implies that given  $\epsilon > 0$ , there exists  $r_\epsilon < r'_0$  such that for  $y \in N(q_0, r_\epsilon)$ , and  $\hat{\lambda}^{(m)} \in \left( \bigcup_{k=1}^K N(\hat{\lambda}_k^{(m)}, r_k) \right)$ ,

$$\left| \frac{1}{\left| J_Q^{(m)}(h(\hat{\lambda}^{(m)}, q_0), \hat{\lambda}^{(m)}) \right|} - \frac{1}{\left| J_Q^{(m)}(h(\hat{\lambda}^{(m)}, q), \hat{\lambda}^{(m)}) \right|} \right| < \epsilon.$$

Thus,

$$\begin{aligned} &\int_{\pi_{\hat{m}}(\Lambda \cap Q^{-1}(q_0))} \left| \frac{1}{\left| J_Q^{(m)}(h(\hat{\lambda}^{(m)}, q_0), \hat{\lambda}^{(m)}) \right|} - \frac{1}{\left| J_Q^{(m)}(h(\hat{\lambda}^{(m)}, q), \hat{\lambda}^{(m)}) \right|} \right| d\hat{\lambda}^{(m)} \\ &\quad \leq \hat{\mu}^{(m)}(\pi_{\hat{m}}(\Lambda \cap Q^{-1}(q_0))) \epsilon \end{aligned}$$

For the second term, we need  $\hat{\mu}^{(m)}(B)$  to be small when  $q$  is close to  $q_0$ . Since  $\{\pi_{\hat{m}}(N(\hat{\lambda}_\ell^{(m+1)}, r'_\ell) \times N(\lambda_\ell^{(m)}, r'_\ell) \times N(\lambda_{\ell j}, r'_\ell)) = N(\hat{\lambda}_\ell^{(m+1)}, r'_\ell) \times N(\lambda_{\ell j}, r'_\ell)\}$  covers  $\pi_{\hat{m}}(\partial\Lambda \cap Q^{-1}(q))$  when  $q \in N(q_0, r'_0)$ , then

$$\hat{\mu}^{(m)}(B) = \hat{\mu}^{(m)}(\pi_{\hat{m}}(\Lambda \cap Q^{-1}(q_0)) \Delta \pi_{\hat{m}}(\Lambda \cap Q^{-1}(q)))$$

$$\leq \sum_{\ell=1}^L \hat{\mu}^{(m)} \left( \left( \pi_{\hat{m}}(\Lambda \cap Q^{-1}(q_0)) \Delta \pi_{\hat{m}}(\Lambda \cap Q^{-1}(q)) \right) \cap \left( N(\hat{\lambda}_\ell^{(m+1)}, r'_\ell) \times N(\lambda_{\ell j}, r'_\ell) \right) \right),$$

and

$$\begin{aligned} \hat{\mu}^{(m)} \left( \left( \pi_{\hat{m}} \left( \Lambda \cap Q^{-1}(q_0) \right) \Delta \pi_{\hat{m}} \left( \Lambda \cap Q^{-1}(q) \right) \right) \cap \left( N(\hat{\lambda}_\ell^{(m+1)}, r'_\ell) \times N(\lambda_{\ell j}, r'_\ell) \right) \right) \\ \leq \int_{N(\hat{\lambda}_\ell^{(m+1)}, r'_\ell)} \left| g(\hat{\lambda}_\ell^{(m+1)}, q_0) - g(\hat{\lambda}_\ell^{(m+1)}, q) \right| d\hat{\lambda}^{(m+1)}. \end{aligned}$$

By the uniform continuity of  $g$ , there exists an  $r'_\ell \leq r'_0$  such that for all  $q \in N(q_0, r'_\ell)$ ,  $\hat{\mu}^{(m)}(B) < \epsilon$ . Finally, we have for all  $y \in N(q_0, r)$ ,  $r = \min(r_\ell, r'_\ell)$ ,

$$\begin{aligned} & |\tilde{\rho}_{\mathcal{D}}(q_0) - \tilde{\rho}_{\mathcal{D}}(y)| \\ & \leq \int_{\pi_{\hat{m}}(\Lambda \cap Q^{-1}(q_0))} \left| \frac{1}{J_Q^{(m)}(h(\hat{\lambda}^{(m)}, q_0), \hat{\lambda}^{(m)})} - \frac{1}{J_Q^{(m)}(h(\hat{\lambda}^{(m)}, q), \hat{\lambda}^{(m)})} \right| d\hat{\lambda}^{(m)} \\ & \quad + \int_B M d\hat{\lambda}^{(m)} \\ & \leq \hat{\mu}^{(m)}(\pi_{\hat{m}}(\Lambda \cap Q^{-1}(q_0))) \epsilon + M\epsilon. \end{aligned}$$

So  $\tilde{\rho}_{\mathcal{D}}(q)$  is continuous at  $q_0$ . Furthermore, the two conditions hold for all  $q$  in  $N(q_0, r'_0)$ , so  $\tilde{\rho}_{\mathcal{D}}(q)$  is continuous in  $N(q_0, r)$  as well.  $\square$

We remove the requirement that  $Q^{-1}(q_0)$  is uniformly parameterized to prove Theorem 2.12.

*Proof of Theorem 2.12.* For all  $\lambda \in Q^{-1}(q_0)$ , there exists a  $N(\lambda, r)$  such that there exists  $\{i_1, \dots, i_m\} \subset \{1, \dots, n\}$  with  $J_Q^{(m)} = (J_Q^{(i_1)} J_Q^{(i_2)} \dots J_Q^{(i_m)})$  being full rank on  $Q^{-1}(q_0)$  in  $N(\lambda, r)$ . The boundary of  $N(\lambda, r) \cap \Lambda$ , which is the union of part of  $\partial\Lambda$  and part of  $\partial N(\lambda, r)$  is piecewise smooth. Suppose  $\partial(N(\lambda, r) \cap \Lambda)$  is locally determined by  $B'(\lambda) = 0$ . When  $r$  is sufficiently small,  $(J_Q \ J_{B'})^\top$  is full rank on  $\partial(N(\lambda, r) \cap \Lambda) \cap Q^{-1}(q_0)$  by continuity of  $J_Q$ . The collection  $\{N(\lambda, r)\}$  admits a finite sub cover  $\{N(\lambda_k, r_k)\}_{k=1}^K$  of  $\Lambda \cap Q^{-1}(q_0)$ . Taking  $r$  sufficiently small, the collection covers  $\Lambda \cap Q^{-1}(q)$ , for  $q$  in  $N(q_0, r)$ . Define  $N_k = N(\lambda_k, r_k) \setminus \left( \bigcup_{j=1}^{k-1} N(\lambda_j, r_j) \right)$ , the boundary of  $N_k \cap \Lambda$  is piecewise smooth. Suppose  $\partial(N_k \cap \Lambda)$  is locally determined by  $B_k(\lambda) = 0$ , then,  $(J_Q \ J_{B_k})^\top$  is full rank on  $\partial(N_k \cap \Lambda)$ , and

$$\tilde{\rho}_{\mathcal{D}}(q) = \int_{Q^{-1}(q) \cap \Lambda} \frac{1}{\sqrt{\det(J_Q J_Q^\top)}} ds = \sum_{k=1}^K \int_{Q^{-1}(q) \cap (N_k \cap \Lambda)} \frac{1}{\sqrt{\det(J_Q J_Q^\top)}} ds.$$

So for all  $q \in N(q_0, r)$ ,

$$|\tilde{\rho}_{\mathcal{D}}(q) - \tilde{\rho}_{\mathcal{D}}(q_0)| \leq \sum_{k=1}^K \left| \int_{Q^{-1}(q) \cap (N_k \cap \Lambda)} \frac{1}{\sqrt{\det(J_Q J_Q^\top)}} ds - \int_{Q^{-1}(q_0) \cap (N_k \cap \Lambda)} \frac{1}{\sqrt{\det(J_Q J_Q^\top)}} ds \right|$$

Theorem A.3 implies that  $\tilde{\rho}_{\mathcal{D}}(q)$  is continuous at  $q_0$ . Since  $\int_{Q^{-1}(q) \cap (N_k \cap \Lambda)} \frac{1}{\sqrt{\det(J_Q J_Q^\top)}} ds$  is continuous in a neighborhood of  $q_0$ ,  $\tilde{\rho}_{\mathcal{D}}(q)$  is continuous in a neighborhood of  $q_0$ .  $\square$

### A.5. Proof of Theorem 3.2

We begin by developing and analyzing numerical solution method for the SIP built on simple function approximations of the integrals in the disintegration (2.5) associated with sequences of partitions of  $\Lambda$  and  $\mathcal{D}$  where random sampling is used to create the partitions. This forms the theoretical basis for the practical sampling-based method used in practice. The approach is heavily influenced by the theory of stochastic geometry and the approximation of sets [46, 57, 68].

We recall fundamental material about approximating the measure of a set using a partition consisting of smaller sets and the approximation of probability density functions using stochastic partitions generated from a Poisson point process. The following is an immediate consequence of the results in [57].

**Theorem A.4.** *Let  $\{\{\omega_j^{(\ell)}\}_{j=1}^{M_\ell}\}_{\ell=1}^\infty$  denote a sequence of random samples generated by a Poisson point process corresponding to a probability measure that has an a.e. positive density function with respect to the Lebesgue measure. If  $A \in \mathcal{B}_\Omega$  satisfies  $\mu_\Omega(\partial A) = 0$ , then*

$$\lim_{\ell \rightarrow \infty} \mu_\Omega(A_{M_\ell} \Delta A) = 0 \text{ a.e.} \quad (\text{A.4})$$

The approximation result (A.4) also holds for sequences of partitions of  $\Omega$  comprising open or closed generalized rectangles with fixed aspect ratios and open balls by standard measure theory results [4, 32]. In those cases, we define the associated sequences of samples using the center of mass of the rectangles or balls.

For an integrable non-negative function  $\rho_\Omega$  defined on  $(\Omega, \mathcal{B}_\Omega, \mu_\Omega)$ , the formal approximation tool is the simple function defined with respect to a given measurable disjoint partition  $\mathcal{I} = \{I_i\}_{i=1}^M \subset \mathcal{B}_\Omega$  of  $\Omega$ ,

$$\rho_{\Omega, M}(\omega) = \sum_{i=1}^M p_i \chi_{I_i}(\omega), \quad p_i = \frac{\int_{I_i} \rho_\Omega d\mu_\Omega}{\int_{I_i} d\mu_\Omega}. \quad (\text{A.5})$$

In practice, we employ estimates of the coefficients  $p_i$  computed using random sampling.

We explore important properties of sequences of approximations associated with sequences of partitions that become finer. We assume that any cell in a partition has negligible boundary, i.e.,  $\mu_\Omega(\partial I_i) = 0$  for all  $i$ . This holds for Voronoi tessellations corresponding to a Poisson process as well as partitions comprising balls and generalized rectangles. We define the **diameter** of a set  $A$  to be  $\text{diam}(A) = \sup_{\omega_1, \omega_2 \in A} \|\omega_1 - \omega_2\|$ , with  $\|\cdot\|$  denoting the Euclidean norm. We consider a sequence of partitions  $\{\mathcal{I}_\ell\}_{\ell=1}^\infty = \{\{I_i^{(\ell)}\}_{i=1}^{M_\ell}\}_{\ell=1}^\infty$ , where  $0 < M_1 < M_2 < \dots$  is a sequence of positive integers. We define  $\text{diam}(\mathcal{I}_\ell) = \max_{1 \leq i \leq M_\ell} \text{diam}(I_i^{(\ell)})$ .

We have the following result.

**Theorem A.5.** *Assume the sequence  $\{\mathcal{I}_\ell\}_{\ell=1}^\infty$  of measurable disjoint partitions of  $\Omega$  satisfy  $\lim_{\ell \rightarrow \infty} \text{diam}(\mathcal{I}_\ell) = 0$ . Then, the family  $\{\rho_{\Omega, M_\ell}\}_{\ell=1}^\infty$  is uniformly integrable and  $\lim_{\ell \rightarrow \infty} \rho_{\Omega, M_\ell} = \rho_\Omega$  a.e.*

*Proof.* We set  $\partial \mathcal{I} = \bigcup_{\ell=1}^\infty \bigcup_{i=1}^{M_\ell} \partial I_i^{(\ell)}$ . If  $\omega \in \Omega \setminus \partial \mathcal{I}$ , the Lebesgue Differentiation Theorem implies that  $\rho_{\Omega, M_\ell}(\omega) \rightarrow \rho_\Omega(\omega)$  as  $\ell \rightarrow \infty$ . The approximation result follows immediately since  $\mu_\Omega(\partial \mathcal{I}) = 0$ .

We next show that  $\{\rho_{\Omega, M_\ell}\}_{\ell=1}^\infty$  is uniformly integrable. For any  $\epsilon > 0$ , there exists an  $\eta$  such that  $\int_{\{\rho_\Omega > \eta\}} \rho_\Omega d\mu_\Omega < \epsilon$ . Let  $\delta = \int_{\{\rho_\Omega > \eta\}} d\mu_\Omega = \mu_\Omega(\{\rho_\Omega > \eta\})$ . Since  $\rho_{\Omega, M_\ell}$  is a simple function, there is a  $\eta'$  such that  $\mu_\Omega(\{\rho_{\Omega, M_\ell} \leq \eta'\}) \geq \delta$  and  $\mu_\Omega(\{\rho_{\Omega, M_\ell} > \eta'\}) < \delta$ . We define  $A_{M_\ell} = \{\rho_{\Omega, M_\ell} > \eta'\} \cup B_{M_\ell}$ , where  $B_{M_\ell}$  is any measurable set satisfying  $B_{M_\ell} \subset \{\rho_{\Omega, M_\ell} = \eta'\}$  and  $\mu_\Omega(B_{M_\ell}) \leq \delta - \mu_\Omega(\{\rho_{\Omega, M_\ell} > \eta'\})$ .

For all  $C \in \mathcal{B}_\Omega$  such that  $\mu_\Omega(C) \leq \delta$ ,

$$\int_C \rho_{\Omega, M_\ell} d\mu_\Omega \leq \int_{A_{M_\ell}} \rho_{\Omega, M_\ell} d\mu_\Omega \leq \int_{\{\rho_{\Omega, M_\ell} > \eta'\}} \rho_{\Omega, M_\ell} d\mu_\Omega + \mu_\Omega(B_{M_\ell}) \eta'. \quad (\text{A.6})$$

By definition, we have

$$\int_{\{\rho_{\Omega, M_\ell} > \eta'\}} \rho_{\Omega, M_\ell} d\mu_\Omega = \int_{\{\rho_{\Omega, M_\ell} > \eta'\}} \rho_\Omega d\mu_\Omega, \quad \int_{\{\rho_{\Omega, M_\ell} = \eta'\}} \rho_\Omega d\mu_\Omega = \mu_\Omega(\{\rho_{\Omega, M_\ell} = \eta'\}) \eta'.$$

There is an  $B'_{M_\ell} \subset \{\rho_{\Omega, M_\ell} = \eta'\}$ , such that  $\mu_\Omega(B'_{M_\ell}) = \mu_\Omega(B_{M_\ell})$  and  $\int_{B'_{M_\ell}} \rho_\Omega d\mu_\Omega \geq \mu_\Omega(B_{M_\ell}) \eta'$ . So (A.6) implies

$$\int_{\{\rho_{\Omega, M_\ell} > \eta'\}} \rho_{\Omega, M_\ell} d\mu_\Omega + \mu_\Omega(B_{M_\ell}) \eta' \leq \int_{\{\rho_{\Omega, M_\ell} > \eta'\}} \rho_\Omega d\mu_\Omega + \int_{B'_{M_\ell}} \rho_\Omega d\mu_\Omega.$$

Since  $\mu_\Omega(\{\rho_{\Omega, M_\ell} > \eta'\} \cup B'_{M_\ell}) = \delta = \mu_\Omega(\{\rho_\Omega > \eta\})$ , we have

$$\int_{\{\rho_{\Omega, M_\ell} > \eta'\}} \rho_\Omega d\mu_\Omega + \int_{B'_{M_\ell}} \rho_\Omega d\mu_\Omega \leq \int_{\{\rho_\Omega > \eta\}} \rho_\Omega d\mu_\Omega < \epsilon$$

□

The foundation of the approximation of the solution of the SIP are sequences of simple functions corresponding to sequences of partitions of  $\mathcal{D}$  and  $\Lambda$ . For a sequence of integers  $0 < M_1 < M_2 < \dots$ , we consider partitions  $\{\mathcal{I}_{M_\ell}\}_{\ell=1}^\infty$  of  $\mathcal{D}$ , with  $\mathcal{I}_{M_\ell} = \{I_i^{(\ell)}\}_{i=1}^{M_\ell}$  and associated points  $\{d_i^{(\ell)}\}_{i=1}^{M_\ell}$ , with  $d_i^{(\ell)} \in I_i^{(\ell)}$  for all  $i, \ell$ . Likewise, for a sequence of integers  $0 < N_1 < N_2 < \dots$ , we consider partitions  $\{\mathcal{T}_{N_j}\}_{j=1}^\infty$  of  $\Lambda$ , with  $\mathcal{T}_{N_j} = \{B_i^{(j)}\}_{i=1}^{N_j}$  and associated points  $\{\lambda_i^{(j)}\}_{i=1}^{N_j}$ , with  $\lambda_i^{(j)} \in B_i^{(j)}$  for all  $i, j$ .

The abstract approximation result is the following.

**Theorem A.6.** *Assume Assumptions 2.1, 2.5, 2.7, 2.8, 2.11, and 3.1 hold and assume the densities  $\rho_p$  and  $\rho_{\mathcal{D}}$  are continuous a.e. There exists a sequence of approximations  $P_{\Lambda, M_\ell, N_j}$  constructed from simple functions and requiring only calculations of measures of cells in the partitions  $\{\mathcal{I}_{M_\ell}\}_{\ell=1}^\infty$  and  $\{\mathcal{T}_{N_j}\}_{j=1}^\infty$  such that*

$$P_\Lambda(A) = \lim_{\ell \rightarrow \infty} \lim_{j \rightarrow \infty} P_{\Lambda, M_\ell, N_j}(A_{N_j}), \quad (\text{A.7})$$

for all sets  $A \in \mathcal{B}_\Lambda$  with  $\mu_\Lambda(\partial A) = 0$ .

We emphasize that the order of the limits in (A.7) is important. As the cells in the partitions of  $\mathcal{D}$  become finer, their inverse images in  $\Lambda$  become “narrower”, and the cells partitioning  $\Lambda$  must also become finer for convergence to hold.

The formal approximation treated in Theorem A.6 is impractical in general because computing the measures of cells in the partitions  $\{\mathcal{I}_{M_\ell}\}_{\ell=1}^\infty$  and  $\{\mathcal{T}_{N_j}\}_{j=1}^\infty$  is computationally untenable. However, the result clarifies the need for the assumptions on the samples used in the numerical solution.

*Proof.* To simplify notation, we prove the result in the case of the uniform prior and drop superscripts  $(\ell)$  and  $(J)$  and subscripts  $\ell$  and  $J$  indicating dependency on the index of  $\{M_\ell\}$  and  $\{N_J\}$  where possible without introducing confusion. We build the approximation in stages. We begin by discussing the approximation of densities.

Since  $\mu_{\mathcal{D}}$  and  $\tilde{\mu}_{\mathcal{D}}$  are equivalent with  $d\tilde{\mu}_{\mathcal{D}} = \tilde{\rho}_{\mathcal{D}} d\mu_{\mathcal{D}}$ ,  $P_{\mathcal{D}}$  has a density  $\rho'_{\mathcal{D}} = \frac{\rho_{\mathcal{D}}}{\tilde{\rho}_{\mathcal{D}}}$  with respect to  $\tilde{\mu}_{\mathcal{D}}$ . We define the simple function,

$$\rho'_{\mathcal{D}, M_\ell} = \sum_{i=1}^{M_\ell} p'_i \chi_{(I_i)}(y), \quad p'_i = \frac{P_{\mathcal{D}}(I_i)}{\tilde{\mu}_{\mathcal{D}}(I_i)} = \frac{\int_{I_i} \frac{\rho_{\mathcal{D}}}{\tilde{\rho}_{\mathcal{D}}} d\tilde{\mu}_{\mathcal{D}}}{\int_{I_i} d\tilde{\mu}_{\mathcal{D}}},$$

as an approximation of  $\tilde{\rho}_{\mathcal{D}}$ . We also define,

$$\rho_{\Lambda, M_\ell} = \sum_{i=1}^{M_\ell} p'_i \chi_{Q^{-1}(I_i)}(\lambda), \quad p'_i = \frac{\int_{I_i} \frac{\rho_{\mathcal{D}}}{\tilde{\rho}_{\mathcal{D}}} d\tilde{\mu}_{\mathcal{D}}}{\int_{I_i} d\tilde{\mu}_{\mathcal{D}}} = \frac{P_{\mathcal{D}}(I_i)}{\tilde{\mu}_{\mathcal{D}}(I_i)} = \frac{P_{\mathcal{D}}(I_i)}{\mu_{\Lambda}(Q^{-1}(I_i))},$$

as an approximation of  $\rho_{\Lambda}$ . By definition,  $\rho_{\Lambda, M_\ell}(\lambda) = \rho'_{\mathcal{D}, M_\ell}(Q(\lambda))$ . By Theorem A.5,  $\rho'_{\mathcal{D}, M_\ell}$  converges to  $\rho'_{\mathcal{D}} = \frac{\rho_{\mathcal{D}}}{\tilde{\rho}_{\mathcal{D}}}$ ,  $\tilde{\mu}_{\mathcal{D}}$ -a.e., so  $\rho_{\Lambda, M_\ell} \rightarrow \rho_{\Lambda}$ ,  $\mu_{\Lambda}$ -a.e., where  $\rho_{\Lambda}(\lambda) = \frac{\rho_{\mathcal{D}}(Q(\lambda))}{\tilde{\rho}_{\mathcal{D}}(Q(\lambda))}$  is the density for the uniform prior solution.

Next, we construct the simple function approximations for the inner integral in the disintegration. The approximation of  $\rho_{\Lambda, M_\ell}$  is defined,

$$\rho_{\Lambda, M_\ell, N_J} = \sum_{j=1}^{N_J} p_j \chi_{B_j}(\lambda), \quad p_j = \frac{P_{\mathcal{D}}(I_i)}{\sum_{Q(\lambda_k) \in I_i} \mu_{\Lambda}(B_k)} \text{ if } \lambda_j \in Q^{-1}(I_i).$$

Theorem A.4 implies  $\sum_{k: Q(\lambda_k) \in I_i} \mu_{\Lambda}(B_k) \rightarrow \mu_{\Lambda}(Q^{-1}(I_i))$ . Theorem A.5 implies  $\rho_{\Lambda, M_\ell, N_J}(\lambda) \rightarrow \rho_{\Lambda, M_\ell}(\lambda)$  as  $J \rightarrow \infty$  for almost all  $\lambda \in \text{int}(Q^{-1}(I_i))$  for some  $I_i \in \mathcal{I}_{M_\ell}$  and therefore  $\rho_{\Lambda, M_\ell, N_J} \rightarrow \rho_{\Lambda, M_\ell}$  a.e. as  $J \rightarrow \infty$ .

Actually, the convergence of  $\rho_{\Lambda, M_\ell, N_J}$  to  $\rho_{\Lambda, M_\ell}$  is uniform. Given  $\epsilon > 0$ , for every  $I_i \in \mathcal{I}_{M_\ell}$ , we choose  $M_J$  sufficiently large to guarantee

$$\mu_{\Lambda} \left( \left( \bigcup_{\lambda_j \in Q^{-1}(I_i)} B_j \right) \Delta Q^{-1}(I_i) \right) < \epsilon.$$

Thus, we can ensure that  $|p_j - p'_i| < \epsilon$  for any  $j$  with  $\lambda_j \in Q^{-1}(I_i)$ . The assumptions imply that

$$|\rho_{\Lambda, M_\ell, N_J}(\lambda) - \rho_{\Lambda, M_\ell}(\lambda)| < \epsilon, \text{ for } \lambda \in \Lambda' \subset \Lambda \text{ with } \mu_{\Lambda}(\Lambda \setminus \Lambda') < \epsilon.$$

Consequently,  $|\max \rho_{\Lambda, M_\ell, N_J} - \max \rho_{\Lambda, M_\ell}| < \epsilon$ . Once we fix a resolution for the approximation of  $\rho_{\mathcal{D}}$  by choosing  $M_\ell$ , we have to choose a sufficient number  $N_J$  of sample points in  $\Lambda$  to obtain the maximum possible accuracy. The intuition is that we have to choose sufficient samples in  $\Lambda$  to accurately represent the geometry of the generalized contours, which of course are positioned in the higher dimensional space  $\Lambda$ .

Next, we turn to the approximation result for  $P_{\Lambda}$ . Theorem A.5 implies that the collection of densities  $\{\rho_{\Lambda, M_\ell}\}_{\ell=1}^{\infty}$  is uniformly integrable. For each  $M_\ell$ , we show  $\{\rho_{\Lambda, M_\ell, N_J}\}_{J=1}^{\infty}$  is uniformly integrable. Given  $\epsilon > 0$ , there exists  $\delta > 0$  such that  $\int_C \rho_{\Lambda, M_\ell} d\mu_{\Lambda} < \epsilon$  for all  $C \in \mathcal{B}_{\Lambda}$  satisfying  $\mu_{\Lambda}(C) \leq \delta$ . For  $N_J$  sufficiently large,  $|\rho_{\Lambda, M_\ell, N_J}(\lambda) - \rho_{\Lambda, M_\ell}(\lambda)| < \epsilon/\delta$  for

$\lambda \in \Lambda' \subset \Lambda$  where  $\mu_\Lambda(\Lambda \setminus \Lambda') < \epsilon / (\max \rho_{\Lambda, M_\ell} + \epsilon / \delta)$ , and  $|\max \rho_{\Lambda, M_\ell, N_j} - \max \rho_{\Lambda, M_\ell}| < \epsilon / \delta$ . So

$$\begin{aligned} \int_C \rho_{\Lambda, M_\ell, N_j} d\mu_\Lambda &= \int_{C \cap \Lambda'} \rho_{\Lambda, M_\ell, N_j} d\mu_\Lambda + \int_{C \setminus \Lambda'} \rho_{\Lambda, M_\ell, N_j} d\mu_\Lambda \\ &\leq \int_{C \cap \Lambda'} (\rho_{\Lambda, M_\ell} + \epsilon / \delta) d\mu_\Lambda + \frac{\epsilon}{\max \rho_{\Lambda, M_\ell} + \epsilon / \delta} (\max \rho_{\Lambda, M_\ell} + \epsilon / \delta) \\ &\leq \int_C \rho_{\Lambda, M_\ell} d\mu_\Lambda + \epsilon + \epsilon < 3\epsilon. \end{aligned}$$

for all  $C \in \mathcal{B}_\Lambda$  satisfying  $\mu_\Lambda(C) \leq \delta$ . This shows the desired result.

If  $A \in \mathcal{B}_\Lambda$  satisfies  $\mu_\Lambda(\partial A) = 0$ ,  $A$  is approximated by  $A_{N_j} = \bigcup_{\lambda_j \in A} B_j$ , and  $P_\Lambda(A)$  is approximated by

$$P_{\Lambda, M_\ell, N_j}(A_{N_j}) = \sum_{\lambda_j \in A} P_{\Lambda, M_\ell, N_j}(B_j) = \int_{A_{N_j}} \rho_{\Lambda, M_\ell, N_j} d\mu_\Lambda.$$

We prove  $P_{\Lambda, M_\ell, N_j}(A_{N_j})$  converges to  $P_\Lambda(A)$  in two steps. First, for fixed  $M_\ell$ , the Vitali Convergence Theorem [61] implies

$$\int_\Lambda |\rho_{\Lambda, M_\ell, N_j} \chi_A - \rho_{\Lambda, M_\ell} \chi_A| d\mu_\Lambda \rightarrow 0 \text{ as } j \rightarrow \infty, \quad (\text{A.8})$$

while the uniform integrability of  $\rho_{\Lambda, M_\ell, N_j}$  implies

$$\int_\Lambda |\rho_{\Lambda, M_\ell, N_j} \chi_{A_{N_j}} - \rho_{\Lambda, M_\ell, N_j} \chi_A| d\mu_\Lambda = \int_{A_{N_j} \Delta A} \rho_{\Lambda, M_\ell, N_j} d\mu_\Lambda \rightarrow 0 \text{ as } j \rightarrow \infty. \quad (\text{A.9})$$

Combining (A.8) and (A.9) shows

$$\int_\Lambda |\rho_{\Lambda, M_\ell, N_j} \chi_{A_{N_j}} - \rho_{\Lambda, M_\ell} \chi_A| d\mu_\Lambda \rightarrow 0 \text{ as } j \rightarrow \infty. \quad (\text{A.10})$$

Another application of the Vitali Convergence Theorem implies,

$$\int_\Lambda |\rho_{\Lambda, M_\ell} \chi_A - \rho_\Lambda \chi_A| d\mu_\Lambda \rightarrow 0 \text{ as } \ell \rightarrow \infty. \quad (\text{A.11})$$

Together (A.10) and (A.11) imply,

$$\int_\Lambda |\rho_{\Lambda, M_\ell, N_j} \chi_{A_{N_j}} - \rho_\Lambda \chi_A| d\mu_\Lambda \rightarrow 0 \text{ as } j \rightarrow \infty \text{ and then } \ell \rightarrow \infty,$$

hence  $\lim_{\ell \rightarrow \infty} \lim_{j \rightarrow \infty} \int_{A_{N_j}} \rho_{\Lambda, M_\ell, N_j} d\mu_\Lambda = \int_A \rho_\Lambda d\mu_\Lambda = P_\Lambda(A)$ .  $\square$

We now turn to the main result.

*Proof of Theorem 3.2.*

*Theorem 3.2: Part 1*

We begin by computing,

$$\begin{aligned}
E\left(\frac{\sum_{k=1}^{N_J} \chi_{\lambda_k}(Q^{-1}(I_i^{(K)}) \cap A)}{\sum_{j=1}^{N_J} \chi_{\lambda_j}(Q^{-1}(I_i^{(K)}))}\right) &= \sum_{k=1}^{N_J} E\left(\frac{\chi_{\lambda_k}(Q^{-1}(I_i^{(K)}) \cap A)}{\sum_{j=1}^{N_J} \chi_{\lambda_j}(Q^{-1}(I_i^{(K)}))}\right) \\
&= \sum_{k=1}^{N_J} \check{p}_i^{(K)} \sum_{j=1}^{N_J} \frac{1}{j} \binom{N_J - 1}{j-1} (p_i^{(K)})^{j-1} (1 - p_i^{(K)})^{N_J - j} \\
&= \frac{\check{p}_i^{(K)}}{p_i^{(K)}} \sum_{j=1}^{N_J} \frac{N_J!}{j!(N_J - j)!} (p_i^{(K)})^j (1 - p_i^{(K)})^{N_J - j} \\
&= \frac{\check{p}_i^{(K)}}{p_i^{(K)}} (1 - (1 - p_i^{(K)})^{N_J}). \tag{A.12}
\end{aligned}$$

Then

$$\begin{aligned}
E(\hat{P}_{\Lambda, K, N_J}(A)) &= \sum_{i=1}^{M_K} E\left(\frac{\sum_{j=1}^{N_J} \chi_{\lambda_j}(Q^{-1}(I_i^{(K)}) \cap A)}{\sum_{j=1}^{N_J} \chi_{\lambda_j}(Q^{-1}(I_i^{(K)}))} \cdot \frac{1}{K} \sum_{k=1}^K \chi_{q_k}(I_i^{(K)})\right) \\
&= \sum_{i=1}^{M_K} E\left(\frac{\sum_{j=1}^{N_J} \chi_{\lambda_j}(Q^{-1}(I_i^{(K)}) \cap A)}{\sum_{j=1}^{N_J} \chi_{\lambda_j}(Q^{-1}(I_i^{(K)}))}\right) E\left(\frac{1}{K} \sum_{k=1}^K \chi_{q_k}(I_i^{(K)})\right) \\
&= \sum_{i=1}^{M_K} \frac{\check{p}_i^{(K)}}{p_i^{(K)}} (1 - (1 - p_i^{(K)})^{N_J}) P_{\mathcal{D}}(I_i^{(K)}). \tag{A.13}
\end{aligned}$$

We define a sequence of measurable functions  $\eta_{\mathcal{D}, K}(q) = \sum_{i=1}^{M_K} \frac{\check{p}_i^{(K)}}{p_i^{(K)}} \chi_q(I_i^{(K)})$  on  $\mathcal{D}$ . Disintegration gives

$$\frac{\check{p}_i^{(K)}}{p_i^{(K)}} = \frac{\int_{Q(Q^{-1}(I_i^{(K)}) \cap A)} P_{p, N}(Q^{-1}(I_i^{(K)}) \cap A | q) d\tilde{P}_{p, \mathcal{D}}}{\int_{I_i} d\tilde{P}_{p, \mathcal{D}}} = \frac{\int_{I_i^{(K)}} P_{p, N}(A | q) d\tilde{P}_{p, \mathcal{D}}}{\int_{I_i^{(K)}} d\tilde{P}_{p, \mathcal{D}}}.$$

The Lebesgue Differentiation Theorem implies that  $\eta_{\mathcal{D}, K}(q) \rightarrow P_{p, N}(A | q)$   $P_{\mathcal{D}}$ -a.e. The collection  $\{\eta_{\mathcal{D}, M_K}\}$  is uniform integrable with respect to  $P_{\mathcal{D}}$  so the Vitali Convergence Theorem implies,

$$\int_{\mathcal{D}} |\eta_{\mathcal{D}, K}(q) - P_{p, N}(A | q)| dP_{\mathcal{D}} \rightarrow 0 \text{ and } \lim_{K \rightarrow \infty} \sum_{i=1}^{M_K} \frac{\check{p}_i^{(K)}}{p_i^{(K)}} P_{\mathcal{D}}(I_i^{(K)}) = P_{\Lambda}(A).$$

Combining this with (3.6) yields the result.

*Theorem 3.2: Part 2*

We start with an estimate of the second moment,

$$\begin{aligned}
& E \left( \sum_{i=1}^{M_K} \frac{\sum_{j=1}^{N_J} \chi_{\lambda_j}(Q^{-1}(I_i^{(K)}) \cap A)}{\sum_{j=1}^{N_J} \chi_{\lambda_j}(Q^{-1}(I_i^{(K)}))} \chi_{q_k}(I_i^{(K)}) \right)^2 \\
&= \iint \left( \left( \sum_{i=1}^{M_K} \frac{\sum_{j=1}^{N_J} \chi_{\lambda_j}(Q^{-1}(I_i^{(K)}) \cap A)}{\sum_{j=1}^{N_J} \chi_{\lambda_j}(Q^{-1}(I_i^{(K)}))} \chi_{q_k}(I_i^{(K)}) \right)^2 dP_{\mathcal{D}} \right) dP_{\mathbb{P}} \\
&= \int \sum_{i=1}^{M_K} P_{\mathcal{D}}(I_i^{(K)}) \left( \frac{\sum_{j=1}^{N_J} \chi_{\lambda_j}(Q^{-1}(I_i^{(K)}) \cap A)}{\sum_{j=1}^{N_J} \chi_{\lambda_j}(Q^{-1}(I_i^{(K)}))} \right)^2 dP_{\mathbb{P}} \\
&= \sum_{i=1}^{M_K} P_{\mathcal{D}}(I_i^{(K)}) \left( \sum_{j=1}^{N_J} \int \frac{\chi_{\lambda_j}(Q^{-1}(I_i^{(K)}) \cap A)}{\left( \sum_{j=1}^{N_J} \chi_{\lambda_j}(Q^{-1}(I_i^{(K)})) \right)^2} dP_{\mathbb{P}} \right. \\
&\quad \left. + \sum_{j \neq k}^{N_J} \int \frac{\chi_{\lambda_j^{(j)}, \lambda_k^{(j)}}(Q^{-1}(I_i^{(K)}) \cap A)}{\left( \sum_{j=1}^{N_J} \chi_{\lambda_j}(Q^{-1}(I_i^{(K)})) \right)^2} dP_{\mathbb{P}} \right) \\
&= \sum_{i=1}^{M_K} P_{\mathcal{D}}(I_i^{(K)}) (N_J A_1 + N_J (N_J - 1) A_2). \tag{A.14}
\end{aligned}$$

We first estimate,

$$\begin{aligned}
A_1 &= \sum_{j=1}^{N_J} \frac{1}{j^2} \check{p}_i^{(K)} \binom{N_J - 1}{j - 1} (p_i^{(K)})^{j-1} (1 - p_i^{(K)})^{N_J - j} \\
&\leq \sum_{j=1}^{N_J} \frac{2}{j(j+1)} \check{p}_i^{(K)} \binom{N_J - 1}{j - 1} (p_i^{(K)})^{j-1} (1 - p_i^{(K)})^{N_J - j} \\
&= \frac{2\check{p}_i^{(K)}}{(N_J + 1)N_J(p_i^{(K)})^2} \sum_{j=1}^{N_J} \binom{N_J + 1}{j + 1} (p_i^{(K)})^{j+1} (1 - p_i^{(K)})^{N_J - j} \\
&= \frac{2\check{p}_i^{(K)}}{(N_J + 1)N_J(p_i^{(K)})^2} (1 - (1 - p_i^{(K)})^{N_J} (1 + N_J p_i^{(K)})). \tag{A.15}
\end{aligned}$$

For  $A_2$ ,

$$\begin{aligned}
A_2 &= \sum_{j=2}^{N_J} \frac{1}{j^2} (\check{p}_i^{(K)})^2 \binom{N_J - 2}{j - 2} (p_i^{(K)})^{j-2} (1 - p_i^{(K)})^{N_J - j} \\
&\leq (\check{p}_i^{(K)})^2 \sum_{j=2}^{N_J} \frac{1}{j(j-1)} \binom{N_J - 2}{j - 2} (p_i^{(K)})^{j-2} (1 - p_i^{(K)})^{N_J - j} \\
&= \frac{(\check{p}_i^{(K)})^2}{N_J(N_J - 1)(p_i^{(K)})^2} (1 - (1 - p_i^{(K)})^{N_J-1} (1 + (N_J - 1)p_i^{(K)})). \tag{A.16}
\end{aligned}$$

Combining (3.6), (A.14), (A.15), and (A.16) yields,

$$\begin{aligned}
\text{Var}(\hat{P}_{\Lambda, M_K, N_j}(A)) &= \frac{1}{K^2} \sum_{k=1}^K \text{Var} \left( \sum_{i=1}^{M_K} \frac{\sum_{j=1}^{N_j} \chi_{\lambda_j}(I_i^{(K)} \cap A)}{\sum_{j=1}^{N_j} \chi_{\lambda_j}(Q^{-1}(I_i^{(K)}))} \chi_{q_k}(I_i^{(K)}) \right) \\
&\leq \frac{1}{K} \left( \sum_{i=1}^{M_K} P_{\mathcal{D}}(I_i^{(K)}) \left( \frac{2\check{p}_i^{(K)}}{(N_j + 1)(p_i^{(K)})^2} (1 - (1 - p_i^{(K)})^{N_j}(1 + N_j p_i^{(K)})) \right. \right. \\
&\quad \left. \left. + \frac{(\check{p}_i^{(K)})^2}{(p_i^{(K)})^2} (1 - (1 - p_i^{(K)})^{N_j-1}(1 + (N_j - 1)p_i^{(K)})) \right) \right. \\
&\quad \left. - \left( \sum_{i=1}^{M_K} \frac{\check{p}_i^{(K)}}{p_i^{(K)}} (1 - (1 - p_i^{(K)})^{N_j}) P_{\mathcal{D}}(I_i^{(K)}) \right)^2 \right). \quad (\text{A.17})
\end{aligned}$$

This implies (3.7) and the convergence result.

*Theorem 3.2: Part 3*

By the Law of Large Numbers,

$$\lim_{J \rightarrow \infty} \frac{\sum_{j=1}^{N_j} \chi_{\lambda_j}(Q^{-1}(I_i^{(K)}) \cap A)}{\sum_{j=1}^{N_j} \chi_{\lambda_j}(Q^{-1}(I_i^{(K)}))} = \frac{P_p(Q^{-1}(I_i^{(K)}) \cap A)}{P_p(Q^{-1}(I_i^{(K)}))} \quad \text{a.e.}$$

We write,

$$\begin{aligned}
\lim_{J \rightarrow \infty} \hat{P}_{\Lambda, M_K, N_j}(A) &= \sum_{i=1}^{M_K} \frac{\check{p}_i^{(K)}}{p_i^{(K)}} \cdot \frac{1}{K} \sum_{k=1}^K \chi_{q_k}(I_i^{(K)}) \\
&= \sum_{i=1}^{M_K} \frac{\check{p}_i^{(K)}}{p_i^{(K)}} \left( \frac{1}{K} \sum_{k=1}^K \chi_{q_k}(I_i^{(K)}) - P_{\mathcal{D}}(I_i^{(K)}) \right) + \sum_{i=1}^{M_K} \frac{\check{p}_i^{(K)}}{p_i^{(K)}} P_{\mathcal{D}}(I_i^{(K)}). \quad (\text{A.18})
\end{aligned}$$

(3.6) implies that  $\sum_{i=1}^{M_K} \frac{\check{p}_i^{(K)}}{p_i^{(K)}} P_{\mathcal{D}}(I_i^{(K)}) \rightarrow P_{\Lambda}(A)$  a.e. We set,

$$\begin{aligned}
&\sum_{i=1}^{M_K} \frac{\check{p}_i^{(K)}}{p_i^{(K)}} \left( \frac{1}{K} \sum_{k=1}^K \chi_{q_k}(I_i^{(K)}) - P_{\mathcal{D}}(I_i^{(K)}) \right) \\
&= \frac{1}{K} \sum_{k=1}^K \left( \sum_{i=1}^{M_K} \frac{\check{p}_i^{(K)}}{p_i^{(K)}} (\chi_{q_k}(I_i^{(K)}) - P_{\mathcal{D}}(I_i^{(K)})) \right) = \frac{1}{K} \sum_{k=1}^K X_k^{(K)}.
\end{aligned}$$

Since  $\{X_k^{(K)}\}$  is bounded, Hoeffding's inequality implies that for  $\epsilon > 0$ ,

$$\sum_{K=1}^{\infty} P_{\mathcal{D}} \left( \left| \frac{1}{K} \sum_{k=1}^K X_k^{(K)} \right| \geq \epsilon \right) < \infty.$$

The First Borel-Cantelli Lemma implies  $\lim_{K \rightarrow \infty} \frac{1}{K} \sum_{k=1}^K X_k^{(K)} = 0$  a.s. □

### A.6. Proof of results in § 3.4

*Proof of Theorem 3.3.* We define the triangular array,

$$X_k^{(K)} = \sum_{i=1}^{M_K} \frac{\check{p}_i^{(K)}}{p_i^{(K)}} \left( \chi_{q_k}(I_i^{(K)}) - P_{\mathcal{D}}(I_i^{(K)}) \right).$$

We set  $S_K = \sum_{k=1}^K X_k^{(K)}$  and  $s_K^2 = \text{Var}(S_K) = K \text{Var}(X_k^{(K)})$ . We have

$$s_K^2 = K \left( \sum_{i=1}^{M_K} \left( \frac{\check{p}_i^{(K)}}{p_i^{(K)}} \right)^2 P_{\mathcal{D}}(I_i^{(K)}) - \sum_{i=1}^{M_K} \left( \frac{\check{p}_i^{(K)}}{p_i^{(K)}} P_{\mathcal{D}}(I_i^{(K)}) \right)^2 \right)$$

so  $\lim_{K \rightarrow \infty} \frac{s_K^2}{K} = \sigma_p^2$ . Markov's inequality implies that for  $\epsilon > 0$ ,  $P_{\mathcal{D}}(|X_k^{(K)} - E(X_k^{(K)})| > \epsilon s_K) < \frac{1}{\epsilon^2 K}$ . So, Lindeberg's condition,

$$\lim_{K \rightarrow \infty} \frac{1}{s_K^2} \sum_{k=1}^K E \left( (X_k^{(K)} - E(X_k^{(K)}))^2 \chi_{\{|X_k^{(K)} - E(X_k^{(K)})| > \epsilon s_K\}} \right) = 0,$$

is satisfied. The Central Limit Theorem implies  $\frac{1}{s_K} \sum_{k=1}^K X_k^{(K)} \xrightarrow{d} \mathcal{N}(0, 1)$ .  $\square$

*Proof of Theorem 3.4.* From the proof of Theorem 3.2, we know that

$$E(T_{3,i,J}) = -\frac{\check{p}_i^{(K)}}{p_i^{(K)}} ((1 - p_i^{(K)})^{N_J}),$$

and

$$\begin{aligned} \text{Var}(T_{3,i,J}) &= \frac{2\check{p}_i^{(K)}}{(N_J + 1)(p_i^{(K)})^2} (1 - (1 - p_i^{(K)})^{N_J} (1 + N_J p_i^{(K)})) \\ &\quad + \left( \frac{(\check{p}_i^{(K)})^2}{(p_i^{(K)})^2} \right) (1 - (1 - p_i^{(K)})^{N_J - 1} (1 + (N_J - 1) p_i^{(K)})) \\ &\quad - \left( \frac{(\check{p}_i^{(K)})^2}{(p_i^{(K)})^2} \right) (1 - (1 - p_i^{(K)})^{N_J})^2. \end{aligned}$$

The result follows.  $\square$

Both  $E(T_{3,i,J})$  and  $\text{Var}(T_{3,i,J})$  become small as  $J \rightarrow \infty$  because  $(1 - p_i^{(K)})^{N_J}$  becomes small. However,  $p_i^{(K)}$  approaches 0. To bound  $(1 - p_i^{(K)})^{N_J} \leq \epsilon$  for  $\epsilon > 0$ , we need to choose  $N_J$  so

$$N_J \geq \frac{\log(\epsilon)}{\log(1 - p_i^{(K)})} \approx -\frac{\log(\epsilon)}{p_i^{(K)}}.$$

### A.7. Proof of Theorem 3.5

*Proof.* As shown in the proof of *Theorem 3.2: Part 3*, it suffices to show that

$$\sum_{i=1}^{M_K} \frac{\check{p}_i^{(K)}}{p_i^{(K)}} \left( \hat{P}_{\mathcal{D}}(I_i^{(K)}) - P_{\mathcal{D}}(I_i^{(K)}) \right) \rightarrow 0 \quad \text{a.s.} \quad (\text{A.19})$$

We estimate,

$$\begin{aligned} \left| \sum_{i=1}^{M_K} \frac{\check{p}_i^{(K)}}{p_i^{(K)}} \left( \hat{P}_{\mathcal{D}}(I_i^{(K)}) - P_{\mathcal{D}}(I_i^{(K)}) \right) \right| &= \left| \sum_{i=1}^{M_K} \frac{\check{p}_i^{(K)}}{p_i^{(K)}} \left( \int_{I_i^{(K)}} (\hat{\rho}_{\mathcal{D}}(q) - \rho_{\mathcal{D}}(q)) d\mu_{\mathcal{D}}(q) \right) \right| \\ &\leq \sum_{i=1}^{M_K} \int_{I_i^{(K)}} |\hat{\rho}_{\mathcal{D}}(q) - \rho_{\mathcal{D}}(q)| d\mu_{\mathcal{D}}(q) \\ &= \int_{\mathcal{D}} |\hat{\rho}_{\mathcal{D}}(q) - \rho_{\mathcal{D}}(q)| d\mu_{\mathcal{D}}(q). \end{aligned}$$

The result follows by assumption. □